HHS Public Access

Author manuscript

Dev Cell. Author manuscript; available in PMC 2019 April 02.

Published in final edited form as:

Dev Cell. 2018 February 05; 44(3): 378–391.e5. doi:10.1016/j.devcel.2017.12.026.

A Lipid Transfer Protein Signaling Axis Exerts Dual Control of Cell-Cycle and Membrane Trafficking Systems

Jin Huang[1,10], **Carl J. Mousley**[2,10,*], **Louis Dacquay**[3], **Nairita Maitra**[4], **Guillaume Drin**[5], **Chong He**[6], **Neale D. Ridgway**[7], **Ashutosh Tripathi**[1], **Michael Kennedy**[3], **Brian K. Kennedy**[6,8], **Wenshe Liu**[9], **Kristin Baetz**[3], **Michael Polymenis**[4], and **Vytas A. Bankaitis**[1,4,9,11,*]

[1]Department of Molecular and Cellular Medicine, Texas A&M Health Sciences Center, College Station, TX 77843-1114, USA

[2]School of Biomedical Sciences, Curtin Health Innovation Research Institute (CHIRI), Faculty of Health Sciences, Curtin University, Bentley, WA 6102, Australia

[3]Ottawa Institute of Systems Biology, Department of Biochemistry, Microbiology and Immunology, University of Ottawa, Ottawa, ON, Canada

[4]Department of Biochemistry & Biophysics, Texas A&M University, College Station, TX 77843-2128, USA

[5]Université Côte d'Azur, CNRS, Institut de Pharmacologie Moléculaire et Cellulaire, Valbonne, France

[6]Buck Institute for Research on Aging, 8001 Redwood Boulevard, Novato, CA 94945, USA

[7]Departments of Pediatrics and Biochemistry and Molecular Biology, Atlantic Research Centre, Dalhousie University, Halifax, NS B3H 4R2, Canada

[8]Centre for Healthy Ageing, National University Health System and Departments of Biochemistry and Physiology, National University, Singapore, Singapore

[9]Department of Chemistry, Texas A&M University, College Station, TX 77843, USA

[10]These authors contributed equally

[11]Lead Contact

SUMMARY

[*]Correspondence: carl.mousley@curtin.edu.au (C.J.M.), vytas@tamhsc.edu (V.A.B.).

AUTHOR CONTRIBUTIONS

H.J., C.J.M., N.M., L.D., M.K., K.B., W.L., M.P., and V.A.B. designed and performed the genetic, transcriptomic, biochemical, and cell-cycle experiments. G.D. and N.D.R. carried out the lipid extraction and transfer assays. C.H. and B.K.K. performed the replicative lifespan experiments. A.T. analyzed the structural consequences of K_{109} modification. All authors contributed to production of the figures and writing of the manuscript.

SUPPLEMENTAL INFORMATION

Supplemental Information includes seven figures and can be found with this article online at https://doi.org/10.1016/j.devcel.2017.12.026.

DECLARATION OF INTERESTS

The authors declare no competing interests.

Kes1/Osh4 is a member of the conserved, but functionally enigmatic, oxysterol binding protein-related protein (ORP) superfamily that inhibits phosphatidylinositol transfer protein (Sec14)-dependent membrane trafficking through the *trans*-Golgi (TGN)/endosomal network. We now report that Kes1, and select other ORPs, execute cell-cycle control activities as functionally non-redundant inhibitors of the G_1/S transition when cells confront nutrient-poor environments and promote replicative aging. Kes1-dependent cell-cycle regulation requires the Great-wall/MASTL kinase ortholog Rim15, and is opposed by Sec14 activity in a mechanism independent of Kes1/Sec14 bulk membrane-trafficking functions. Moreover, the data identify Kes1 as a non-histone target for NuA4 through which this lysine acetyltransferase co-modulates membrane-trafficking and cell-cycle activities. We propose the Sec14/Kes1 lipid-exchange protein pair constitutes part of the mechanism for integrating TGN/endosomal lipid signaling with cell-cycle progression and hypothesize that ORPs define a family of stage-specific cell-cycle control factors that execute tumor-suppressor-like functions.

Graphical Abstract

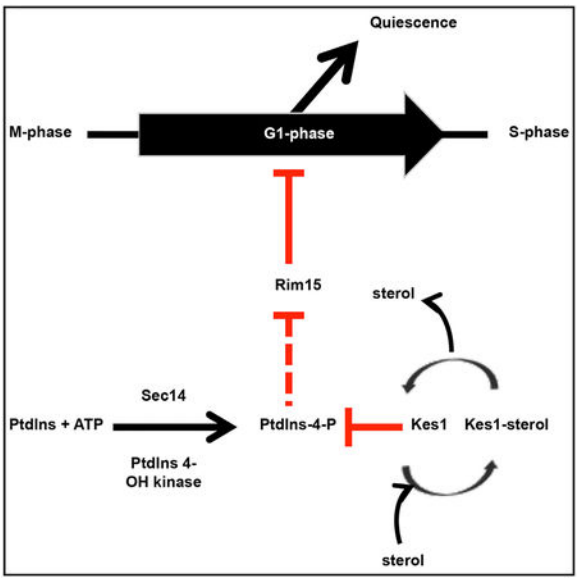

In Brief

Huang et al. demonstrate the yeast oxysterol-binding protein (ORP) homolog Kes1, and other ORPs, are inhibitors of the G_1/S transition. They show that Kes1 is a non-histone target for the NuA4 lysine acetyltransferase and participates in a phosphatidylinositol-4-phopshate-dependent mechanism for integrating TGN/endosomal lipid signaling with cell-cycle progression.

INTRODUCTION

The *trans*-Golgi (TGN) network/endosomal system consists of highly dynamic organelles that sit at the confluence of antero-grade and endocytic membrane flow (Glick and Nakano, 2009). Thus, the TGN/endosomal system serves as an important membrane-sorting station, and as a major node for intracellular signaling. TGN/endosomal signaling programs involve multiple branches of lipid metabolism, with a robust and essential interface between lipid

metabolism and membrane trafficking through these compartments (Bard and Malhotra, 2006; Graham and Burd, 2011).

Lipid exchange proteins play crucial roles in coordinating lipid metabolism with phosphoinositide signaling and membrane trafficking in TGN/endosomes (Bankaitis et al., 1990, 2010; Graham and Burd, 2011). This circuit is controlled by opposing actions of two lipid-exchange proteins: the PtdIns/PtdCho transfer protein Sec14 and Kes1/Osh4 (Fang et al., 1996; Mousley et al., 2012). Sec14 couples PtdCho biosynthesis with PtdIns-4-P production (Cleves et al., 1991; Schaaf et al., 2008). In turn, PtdIns-4-P signaling drives TGN/endosomal trafficking (Graham and Burd, 2011). Kes1 is one of seven yeast oxysterol binding-related proteins (ORPs) (Fang et al., 1996; Beh et al., 2001), and it antagonizes Sec14 activity by sequestering PtdIns-4-P from its pro-trafficking effectors (Li et al., 2002; de Saint-Jean et al., 2011). Recent studies indicate that a Kes1 sterol/PtdIns-4-P exchange cycle controls amplitude of this trafficking “brake” by tuning the ability of Kes1 to sequester PtdIns-4-P (Mousley et al., 2012).

Although conserved across the *Eukaryota*, ORPs remain functionally enigmatic, with conflicting data as to whether ORPs are intermembrane lipid transfer proteins or not (Schulz and Prinz, 2009; Georgiev et al., 2011; Stefan et al., 2011; Mousley et al., 2012). This confusion reflects the lack of information regarding the biological activities of these proteins. Kes1 is the exception. It is not only unique among yeast ORP proteins in its role as antagonist to Sec14-dependent PtdIns-4-P signaling in the TGN/endosomal system, but Kes1 is also an antagonist of nitrogen stress responses and mammalian target of rapamycin complex 1(TORC1) signaling (Mousley et al., 2012). Those results forecast complex physiological functions for Kes1, and identify homeostatic regulation of Kes1 activity as a key point of control at the interface of membrane-trafficking, nutrient signaling, and cell-cycle progression. Issues of how cells coordinate membrane growth and trafficking with nutrient signaling and entry into a new mitotic cycle define fundamental, but poorly understood, questions in contemporary cell biology (McCusker and Kellogg, 2012).

In this study, we characterize Kes1 activity as a negative regulator of progression through the G_1 stage of the cell cycle when cells confront nutrient-prohibitive environments. We further demonstrate that the antagonistic actions of Kes1 and Sec14 in TGN/endosomal membrane trafficking extend to cell-cycle contexts. Strikingly, these cell-cycle involvements are independent of the roles of these proteins in regulating bulk membrane trafficking. Thus, Kes1 and Sec14 execute dual functions in membrane-trafficking and cell-cycle control, and are well positioned to coordinate cell-cycle progression with membrane flux through the TGN/endosomal system. We also show that Kes1 activity is subject to regulation by the NuA4 lysine acetyltransferase (KAT). Together, the data reveal an interface between TGN/endosomal lipid signaling and cell-cycle control, identify the NuA4 KAT complex as a regulator of that interface, and suggest ORPs as stage-specific inhibitors of cell-cycle progression in eukaryotes.

RESULTS

Kes1-Induced Cell-Cycle Arrest Exhibits Signatures of Quiescence

The first *in vivo* clues regarding ORP function came from demonstrations that Kes1 is an antagonist of Sec14 and PtdIns-4-P signaling in the context of membrane trafficking through the TGN-endosomal system. That functional readout is complex, however, as it is Kes1 LOF that restores growth and membrane trafficking to cells deficient in normally essential Sec14 activities (Fang et al., 1996; Li et al., 2002). A simpler context was suggested by Mousley et al. (2012), who demonstrated that excessive Kes1 activity evokes an amino acid remedial growth arrest by attenuating TORC1 signaling. Upon elevation of Kes1 activity, most cells arrest in G_1, as determined by their terminal pheno-type of large unbudded cells with 1N genome content (Figure 1A). Furthermore, G_1 cells with excessive Kes1 activity are unable to initiate a new round of cell division in nutrient-replete media, even though these cells continue to increase their size at a rate similar to that of matched controls, demonstrating that inability to initiate cell division was not due to a general growth deficiency (Figure S1). These collective data forecast a role for Kes1 in the G_1 phase when cells evaluate nutrient cues before committing to another round of cell division.

The MBF/SBF regulon defines a set of genes whose expression is required to negotiate the G_1/S transition or START (Spellman et al., 1998; Zaman et al., 2008). Transcription of multiple genes regulated by MBF and SBF was reduced ≥3-fold relative to control in otherwise wild-type (WT) yeast cells programmed for elevated (and doxycycline-repressible) expression of Kes1 or Kes1^{Y97F} (a dominant-active Kes1 defective in sterol-binding but competent for PtdIns-4-P binding; Im et al., 2005; Mousley et al., 2012). The affected genes included those encoding G_1 cyclins (*CLN1*, *CLN2*, *PCL1*, *PCL2*, *PCL9*), a gene encoding a homeobox transcription factor that promotes early cell-cycle box gene transcription (*YOX1*), and *AXL2* whose product specifies spatial organization of bud emergence from the mother cell during G_1 (Figure 1B). That reduced *AXL2* expression was of physiological significance was validated by the abnormal bipolar budding phenotype exhibited by Kes1-overex-pressing haploid cells (Figure S2A). Bipolar budding is a signature property of diploid yeast with normal Axl2 levels. Reduced transcription of MBF/SBF-controlled genes were not observed in cells expressing the nonfunctional Kes1^{K109A} defective in PtdIns-4-P binding (Li et al., 2002; de Saint-Jean et al., 2011), nor were these observed in cells where *KES1* or *kes1*^{Y97F} transcription was repressed by Dox (Figure 1B).

Reciprocally, Msn2/4- and Gis1-dependent transcriptional responses were activated in yeast with elevated Kes1 activity. Both Kes1- and Kes1^{Y97F}-arrested cells displayed ≥3-fold elevations in Msn2/4 and Gis1 target gene expression relative to control (*HSP12, HSP78, HSP82,* and *HSP104*, and *SSA3*, *GRE1,* and *CTT1*; Figure 1B). Those derangements were not observed in cells expressing Kes1^{K109A}, nor in cells where ectopic *KES1* or *KES1*^{Y97F} expression was repressed by Dox. Activation of the Msn2/4 and Gis1 regulon is a hallmark of cells transitioning into quiescence in response to nutritional stress (Beck and Hall, 1999; Pedruzzi et al., 2000).

Kes1/Kes1^{Y97F}-arrested cells displayed metabolic signatures of quiescent cells as well. The storage carbohydrate glycogen and the stress protectant trehalose accumulate in yeast

transitioning into quiescence (Lillie and Pringle, 1980). Both metabolites precociously accumulated in Kes1- and Kes1^{Y97F}-arrested cells incubated under nutrient-replete conditions, but not in cells expressing Kes1^{K109A} (Figure 1C). Phosphorylated long-chain sphingoid base (LCBP) accumulation is repressed by the Pho85 cyclin, and elevated LCBP represents another metabolic signature of quiescent cells (Lester et al., 2013). Intracellular LCBP levels of both the dihydro- and phyto-classes were dramatically increased in Kes1- and Kes1^{Y97F}-arrested yeast relative to control (Figure S2B). Moreover, quiescent yeast exhibit reinforced cell walls. This property was scored by resistance to zymolyase digestion (Krause and Gray, 2002). Either Kes1- or Kes1^{Y97F}-overexpressing induced zymolyase resistance to cells cultured in nutrient-rich media (Figure 1D). Elevated Kes1^{K109A} expression had no such effect.

Kes1 Antagonizes PKA Signaling

Entry into quiescence requires the balanced downregulation of both TORC1 (NH_4^+-dependent) and protein kinase A ([PKA]; carbohydrate-dependent) pathways for proliferative signaling (Wei et al., 2008). Two readouts confirmed PKA signaling was downregulated in Kes1/Kes1^{Y97F}-arrested yeast. First, PKA-catalyzed phosphorylation of the model substrate choline kinase (Cki1; Ramachandran and Herman, 2011) was reduced in Kes1/Kes1^{Y97F}-arrested cells, but not in cells expressing Kes1^{K109A} (Figure 2A). Second, processing bodies (P-bodies) are sites for storage, degradation and quality control of translationally repressed mRNAs. These structures, marked by Dcp2 and Xrn1, accumulate in cells as cytoplasmic puncta when PKA signaling is depressed (Ramachandran et al., 2011). Elevated Kes1/Kes1^{Y97F} expression (but not of Kes1^{K109A}) induced robust formation and stable maintenance of cytoplasmic Dcp2- and Xrn1-positive P-body puncta (Figure 2B).

Kes1-Chaperoned Entry into Quiescence Is Rim15 Dependent

The Rim15 kinase regulates exit from the cell cycle into quiescence (Cameroni et al., 2004; Swinnen et al., 2006). Ras/PKA, TORC1, and Pho85 cyclin-dependent kinase phosphate-sensing pathways promote cell proliferation, and inhibit entry into quiescence, by attenuating Rim15 activity in response to nutrient availability. If Kes1 operates upstream of Rim15 in the quiescence pathway, Rim15 activity will be required for entry of Kes1/Kes1^{Y97F}-overexpressing cells into quiescence. Indeed, *rim15Δ* cells were resistant to Kes1/Kes1^{Y97F}-overexpression (Figure 2C). Rim15-deficient cells also failed to present the quiescence signatures typically associated with Kes1/Kes1^{Y97F}-mediated growth arrest. That is, neither glycogen nor trehalose accumulated in *rim15Δ* mutants induced for Kes1/Kes1^{Y97F} expression upon withdrawal of Dox from the medium (Figure 2D), and *rim15Δ* mutant cell walls failed to acquire zymolyase resistance (Figure 2E). Steady-state Kes1 and Kes1^{Y97F} levels were appropriately elevated in *rim15Δ* cells after Dox withdrawal.

Cells Lacking Kes1 Are Less Responsive to Nutrient Deprivation Signals

Kes1 loss-of-function (LOF) mutants did not appropriately exit the cell cycle when confronted by nutrient limitation. Whereas *KES1* cells ceased to proliferate upon reaching a density of ca. 1.5×10^8 cells/mL (Figure 3A, 12–48 hr time points), parallel *kes1Δ* cell cultures consistently reached cell densities of ca. 3×10^8 cells/mL (Figure 3A, 12–48 hr time points). Cells lacking Kes1 ultimately arrested, and the DNA content of *kes1Δ* cell

populations in stationary phase exhibited G_1 signatures indistinguishable from those of their isogenic *KES1*$^+$ counterparts (Figure 3B). However, *kes1Δ*-arrested cells were only ~75% of the size of arrested WT cells (Figure 3C). Thus, Kes1-deficient mutants were licensed to initiate one supernumerary round of cell division under nutrient-prohibitive conditions of such severity that cell expansion could no longer be supported.

The supernumerary cell division phenotype of *kes1Δ* cells suggested that Kes1 is part of the quiescence response, which is engaged when yeast are challenged with nutrient deprivation. In support, survey of multiple metabolic signatures of quiescence demonstrated that *kes1Δ* cells were defective in mounting quiescence responses. Relative to WT cells, Kes1-deficient mutants showed ca. 2-fold reductions in the magnitude of glycogen and trehalose accumulation when starved (Figure 3D). Moreover, nutrient-stressed *kes1Δ* cell walls failed to acquire zymolyase resistance (Figure 3E). Chronological lifespan assays also showed *kes1Δ* cells displayed accelerated loss of viability when subjected to chronic nutrient limitation.

Sec14 and Kes1 Function in Cell-Cycle Control in Cycling Cells

Kes1 antagonizes Sec14 and PtdIns-4-P signaling in the context of membrane trafficking through the TGN-endosomal system. Hence, we investigated whether introducing a *sec14*^{ts} allele into *kes1Δ* cells restored their ability to arrest properly in the face of nutrient exhaustion. Indeed, the license to undergo the supernumerary round of cell division in nutrient-prohibitive environments was partially suppressed in *sec14–1*^{ts} *kes1Δ* cells. Notably, this phenotypic suppression was evident for cells cultured at a permissive temperature (30°C), where the *sec14–1*^{ts} gene product retains sufficient activity to support WT kinetics of bulk membrane trafficking through the secretory and TGN/endosomal pathways.

We examined whether the antagonistic relationship between Sec14 and Kes1 was manifested in cycling cells in nutrient-replete medium. During exponential growth in rich media (YPD), *sec14–1*^{ts} cells exhibited doubling times that were ca. 10% longer than those of isogenic *SEC14* cells (108.7 ± 2.2 versus 93.4 ± 1.3 min, $p < 0.05$, Student's t test). This phenotype was reversed by Kes1 LOF, as *sec14–1*^{ts} *kes1Δ* cells exhibited WT population doubling times (92.6 ± 6.4 min). The population doubling time and DNA content of asynchronous and exponentially dividing *kes1Δ* cells did not differ from the corresponding parameters of isogenic *KES1* cells (Figure 4A). However, *kes1Δ* and *sec14–1*^{ts} cells had altered size homeostasis. Compared with WT, *kes1Δ* cells were slightly smaller, while *sec14–1*^{ts} cells were larger (Figure 4B, left). These differences in the population mean cell size were not due to differences in birth size of these strains (Figure 4B, right), and the large cell size of *sec14–1*^{ts} cells was corrected in *sec14–1*^{ts} *kes1*D cells (Figure 4B, left). "Bypass Sec14" mutations that inactivate PtdCho synthesis via the CDP-choline pathway (*pct1Δ*; Cleves et al., 1991) failed to reduce the size of *sec14–1*^{ts} cells (Figure 4B).

Since the decision to initiate a new round of cell division in response to nutrient signaling is exercised in G_1, we examined cell-cycle progression of highly synchronous early-G_1 daughter cells obtained by centrifugal elutriation. This approach holds the advantage that cell-cycle synchrony is achieved without applying arrest and release regimens that uncouple

cell growth from cell division (e.g., shift of *cdc*^{ts} mutants to restrictive temperatures or pheromone arrest). The elutriated early-G_1 cells were allowed to progress in the cell cycle, and evaluated in a time course by scoring the incidence of budded cells, and the volume of cells, with a channelyzer. Since initiation of DNA replication in yeast is coupled to the formation of a bud (Johnston et al., 1977), the critical size is defined as the size at which 50% of the cells in a synchronous population have initiated a new round of cell division. *KES1*$^{+}$ and *kes1Δ* cells increased in size at the same rate (Figure 4C, left), and exhibited the same critical size (Figure 4C, right). However the critical size of *sec14–1*^{ts} cells was larger than that of isogenic WT cells (47.9 ± 2.1 versus 43.9 ± 1.8 fL, p = 0.003, Student's t test; Figure 4C, right). Because *sec14–1*^{ts} mutants increased in size at WT rates at 30°C (Figure 4C, left), but did not commit to divide until cells reached a larger critical size, their G_1 phase was extended. This protracted G_1 phase, in conjunction with the increase in G_2/M DNA content observed for *sec14–1*^{ts} cells (consistent with a second delay in mitosis; data not shown), accounted for the slower doubling time of *sec14*^{ts} cells at 30°C.

A proper coupling between cell growth and division was reestablished in *sec14–1*^{ts} cells by Kes1 LOF, even though *kes1Δ* mutants by themselves had normal critical size and rate of size increase under nutrient-replete conditions. The corrective effects upon Kes1 LOF were specific because loss of Pct1 (i.e., an independent bypass Sec14 condition) failed to restore a proper critical size to *sec14–1*^{ts} cells (Figure 4C, right).

sec14^{ts} Mutant Exhibits an Unusual Cell Size Control Phenotype

The critical size data obtained from synchronously cycling cell cultures suggested *sec14–1*^{ts} cells, despite their normal rates of cell size increase, did not correctly register that they had grown sufficiently to commit to another round of cell division. This defect was visualized by plotting the logarithm of birth size against relative rate of cell size increase in the G_1 phase of the cell cycle (Figure 4D). Such plots relate the coherence of cell size control mechanisms, and the relevant values for *sec14–1*^{ts} mutants were compared with analogous values for a series of mutants analyzed previously (Soma et al., 2014). The increased cell growth requirements of *sec14–1*^{ts} yeast for the commitment of these cells to a new round of cell division were clear in such representations of the data. The *sec14–1*^{ts} critical size phenotype was unusual in that mutants in growth control processes (e.g., the *rpl20b* ribosomal protein gene deletion) attain degrees of overall cell growth from birth to START that are indistinguishable from WT cells (Figure 4D). By contrast, the *sec14–1*^{ts} phenotype was qualitatively similar to the delay observed in cells lacking the G_1 cyclin Cln3, and was of at least the same magnitude as that observed upon loss of the Bck2 cell-cycle regulator which acts in parallel with Cln3 (Di Como et al., 1995). This delay was corrected by Kes1 LOF (Figure 4D).

Cell Size and Cell Division Phenotypes Are Associated with Defects in Other ORP Proteins

In addition to Kes1, yeast express three Kes1-like "short" ORPs (Osh5, Osh6, and Osh7) and three "long" versions (Osh1, Osh2, and Osh3). The functional differences between Kes1 and other members of the yeast ORP family were evident in: (1) phenotypic bypass Sec14 contexts (Figures 5A and S3A), and (2) CPY pulse-chase trafficking assays assessing bypass Sec14 pheno-types (Figures 5B and S3B). To determine whether cell-cycle dysregulation

associated with Kes1 LOF was a unique property, we examined cells carrying deficiencies in individual members of the Osh protein family. Again, Kes1 LOF was unique in its ability to restore proper size homeostasis to exponentially growing *sec14–1*^{ts} cells at 30°C, and in reducing mean cell size of exponentially growing cells (Figure 5C).

In other contexts, however, loss of Osh protein function did evoke phenotypes similar to those associated with *kes1Δ*. For example, Osh1, Osh3, Osh6, or Osh7 LOF restored WT doubling times to *sec14–1*^{ts} mutants (Figure S3C). Moreover, as was the case for *kes1Δ* mutants, nutrient-deprived cells lacking any single Osh protein (other than Osh5) inappropriately passed through G_1 into another round of cell division (Figure S3D). Analyses of *osh1Δ* and *osh6Δ* cell size profiles during starvation demonstrated that those cells phenocopied *kes1Δ* cells in their reduced cell size upon arrest. Thus, activities of other Osh proteins in cell proliferation resemble, but are not perfectly redundant with, those of Kes1. That Osh5 showed no functional relatedness to Kes1 was of note given it is the closest Kes1 homolog as defined by primary sequence identity/similarity.

Kes1 and Long ORP Defects Extend Replicative Lifespan

As cells deficient in activities of Kes1 or the other Osh proteins (other than Osh5) showed G_1 control defects, we determined the effects of Kes1 LOF and of other Osh protein deficiencies on broader aspects of cell aging and longevity. Those parameters were interrogated in the context of replicative lifespan, i.e., the number of divisions mother cells undergo before reaching senescence. Kes1 LOF extended the mean and maximal replicative lifespan of cells continuously cultured in nutrient-replete media (Figure 5D). In those experiments, the WT strain exhibited a replicative lifespan of 27.7 generations, whereas the *kes1*D derivative exhibited an extended replicative lifespan (35.4 generations). LOF of any one of the three other “short” Kes1-like yeast ORPs had no such effect (Figure 5D). However, LOF of any one of the three “long” ORPs extended replicative lifespan (Figure 5E). Moreover, the small cell size of *kes1* mutants is consistent with those of other long-lived mutants with extended replicative lifespan (He et al., 2014). These findings suggest a trade-off between chronological and replicative lifespan assays for Kes1 activity. That is, Kes1 LOF mutants carry greater replicative potential, but are impaired in their ability to enter a growth-arrested state conducive to long chronological lifespan.

Acetylation of Kes1 Residue K_{109} Inactivates Lipid Exchange *In Vitro*

Kes1 involvement as a physiological brake on progression through START raises questions regarding how Kes1 activity is itself regulated. Two independent profiling studies of the yeast acetylome identify Kes1 as a protein modified at as many as nine lysine residues (Figure 6A; Henriksen et al., 2012; Madsden et al., 2015). To assess the significance of each modification, Ala was substituted for each acetylated Kes1 Lys residue, and the activity of each protein was evaluated in a bypass Sec14 complementation assay, where Kes1 LOF permits growth of *sec14*^{ts} cells at 37°C. K_{109} was the only site for which an Ala substitution ablated Kes1 activity in cells (Figure 6A). This defect was not for trivial reasons as Kes1^{K109A} is a stable protein *in vivo* (Li et al., 2002). The K_{109} acetylation was of special interest because K_{109}: (1) sits within the invariant motif that defines the ORP super-family (Figure 6A; Li et al., 2002), and (2) forms a critical contact with the PtdIns-4-P molecule

that occupies the Kes1 lipid-binding pocket (Figure 6B; de Saint-Jean et al., 2011). Thus, K_{109} acetylation potentially compromises the Kes1::PtdIns-4-P interaction.

To determine the effect of K_{109} acetylation on PtdIns-4-P binding, Kes1^{AcK109} was purified, and the site-specific acetylation was confirmed (Figure S4). Kes1 proteins carrying the inactivating $K_{109}A$, the acetylation-mimetic $K_{109}Q$, and non-acetylatable $K_{109}R$ substitutions were also purified. Activities of those proteins were then assessed in a liposome-based PtdIns-4-P extraction assay. Relative to Kes1, the Kes1^{K109A}, Kes1^{K109Q}, Kes1^{K109R}, and Kes1^{AcK109} proteins all exhibited reduced abilities to extract PtdIns-4-P from liposomes *in vitro* (Figure 6C).

It is not PtdIns-4-P binding/extraction in isolation, rather a heterotypic ergosterol/PtdIns-4-P exchange cycle, that is central to the biochemical mechanism of Kes1 function *in vivo* (Mousley et al., 2012; Moser von Filseck et al., 2015). Thus, the consequences of K_{109} acetylation were also analyzed in dehydroergosterol (DHE)/PtdIns-4-P lipid transfer assays that measure inter-liposomal exchange of those lipids *in vitro* (de Saint-Jean et al., 2011). Indeed, Kes1 was proficient in transfer of both DHE (~9 molecules/Kes1/min) and PtdIns-4-P (~12 molecules/Kes1/min). Kes1^{K109A} and Kes1^{AcK109} were each reduced only ca. 30% for DHE transfer activity relative to Kes1 (Figures 6D and 6E). By contrast, both Kes1^{K109A} and Kes1^{AcK109} exhibited ca. 6-fold reductions in PtdIns-4-P transfer activity. Kes1^{K109Q} was also reduced for PtdIns-4-P transfer (~60% reduction relative to Kes1), although the mutant protein exhibited greater DHE and PtdIns-4-P transfer activity than did Kes1^{AcK109}. Kes1^{K109R} showed a ca. 70% increase in DHE transfer activity, but only modest reduction in PtdIns-4-P transfer activity relative to WT Kes1 (Figures 6D and 6E). Purified Kes1^{K168Q} and Kes1^{K168R} represented controls and were at least as active as Kes1 for DHE and PtdIns-4-P transfer *in vitro* (Figure 6E).

Identifying Candidate KATs that Regulate the Kes1/Sec14 Signaling Axis

The biochemical data indicated that K_{109} acetylation is a viable mechanism for downregulating Kes1 activity *in vivo*, and that KATs and lysine deacetylases are important regulators of the Kes1 DHE/PtdIns-4-P exchange cycle in cells. Two screens identified candidate KATs that regulate Kes1 activity. The first took advantage of the Kes1^{Y97F} PtdIns-4-P clamp whose expression is detrimental to yeast (Mousley et al., 2012). The strategy was to assess the relative toxicity of Kes1^{Y97F} expression to mutants with deficiencies in each of the yeast KATs. Kes1^{Y97F} expression was controlled by a Dox-inducible promoter, and defects in KATs that acetylate K_{109} (i.e., compromise dampening of Kes1 activity) were expected to exacerbate yeast growth sensitivities to Kes1^{Y97F} expression. Whereas all KAT mutants exhibited growth profiles similar to the corresponding controls cultured under non-inducing conditions, the *eaf1Δ*, *rtt109Δ*, and *gcn5Δ* mutants were sensitized to Kes1^{Y97F} expression relative to WT controls (Figure S5A).

The second screen assessed which KAT deficiencies further sensitized *sec14–1^{ts}* mutants to elevated temperatures. Because enhanced Kes1 activity is especially detrimental to growth of *sec14–1^{ts}* mutants (Fang et al., 1996; Li et al., 2002), such a phenotype was expected to be associated with LOF in KAT activities that downregulate Kes1 via K_{109} acetylation. Again, *eaf1Δ* and *rtt109Δ* alleles enhanced the temperature sensitivity of *sec14–1^{ts}* mutants (Figure

S5B). Whereas *gcn5Δ* showed no synthetic effects in this context, *elp3Δ* mutants prohibited growth of *sec14–1*^{ts} cells at 33.5°C. Thus, only *eaf1Δ* and *rtt109Δ* satisfied both of the genetic criteria for KATs that target Kes1 *in vivo*, with *eaf1Δ* consistently showing the most pronounced effects.

Eaf1 is a scaffolding component of the 13-subunit NuA4 KAT complex (Auger et al., 2008). Deficiencies in other subunits of the NuA4 complex also evoked *eaf1Δ*-like phenotypes. The *eaf7Δ* and *esa1*^{ts} (*esa1-L254P*; Clarke et al., 1999) mutations satisfied the dual criteria of rendering WT cells less tolerant of Kes1^{Y97F} toxicity, and enhancing temperature sensitivity for growth of *sec14–1*^{ts} cells (Figure S5C). Moreover, those growth deficits associated with NuA4 deficiencies were alleviated in *kes1*^{0} and *kes1*^{K109A} genetic backgrounds (Figure S5D). Bypass Sec14 mechanisms associated with inactivation of the CDP-choline pathway for PtdCho biosynthesis failed to rescue growth of *sec14–1*^{ts} *eaf1*D double mutants at restrictive temperatures (Figure S5E). These phenotypic data were reinforced by assays monitoring recycling of the Snc1 t-SNARE through the endosomal system to the plasma membrane (Figure S6A), and CPY trafficking through the secretory pathway to the vacuole (Figure S6B). These results identified Kes1 as a key non-histone target of the NuA4 KAT.

Kes1^{K109R} Is Defective *In Vivo*

If Kes1 regulation is a case of the NuA4 KAT complex tuning Kes1 activity via K_{109} acetylation, then the acetylation mimic Kes1^{K168Q} should not be functional *in vivo*. Moreover, expression of a non-acetylatable Kes1 that retains PtdIns-4-P and sterol-binding activities (i.e., Kes1^{K109R}) should phenocopy the G_1-arrest phenotypes that come with enhanced Kes1 or Kes1^{Y97F} expression. The first prediction was fulfilled while the second was not. Whereas Kes1 re-expression reversed the bypass Sec14 phenotype of *kes1* null mutants, Kes1^{K109A}, Kes1^{K109Q}, or Kes1^{K109R} re-expression was not able to do so (Figure S7A), even though these K_{109} mutant proteins were stable *in vivo*. Similar conclusions were forthcoming from pulse-chase experiments where CPY-trafficking kinetics were examined (Figure S7B). Kes1^{K109A}, Kes1^{K109Q}, or Kes1^{K109R} expression did not reverse the bypass Sec14 status of *kes1* null cells. Moreover, in contrast to Kes1 or Kes1^{Y97F}, elevated Kes1^{K109R} did not inhibit growth of WT or *sec14–1*^{ts} strains. Thus, despite the fact that Kes1^{K109R} was nearly as active as the WT protein in a coupled DHE/PtdIns-4-P transfer assay *in vitro*, Kes1^{K109R} was nonfunctional *in vivo*.

DISCUSSION

Understanding how ORPs are integrated into the eukaryotic lipid signaling program requires a description of their individual biological activities. Herein, we identify a role for Kes1, and other ORPs, in regulating cell-cycle progression and replicative lifespan in yeast. Those findings outline four conclusions: (1) Kes1 functions as a key brake on progression through G_1 and initiation of a new round of cell division upon nutrient limitation, (2) the antagonistic actions of Kes1 and Sec14 in regulating PtdIns-4-P signaling extend from membrane trafficking to cell-cycle contexts where the Sec14/Kes1 lipid signaling axis plays an important role in coordinating cell growth with initiation of cell division in nutrient-replete environments, (3) Kes1 is a key nonhistone target for acetylation by the NuA4 lysine

acetyltransferase, and (4) other members of the yeast ORP family also exhibit activities consistent with stage-specific inhibitors of cell-cycle progression and regulators of replicative lifespan. These data report that Kes1 and Sec14 execute dual membrane-trafficking and cell-cycle functions, and nominate this pair of lipid-exchange proteins as components of a regulatory axis that coordinates TGN/endosomal lipid signaling with cell-cycle progression. Moreover, these results offer fresh perspectives for interpreting ORP function in cell-cycle control, and suggest that ORPs execute unappreciated “tumor-suppressor”-like activities in mammalian cells.

Kes1 Promotes Exit from the Cell Cycle into Quiescence

Kes1 action as an inhibitor of progression through G_1 is manifested by excessive Kes1 activity overriding the nutrient-responsive pro-proliferative signals that drive progression through G_1 into another round of cell division and, reciprocally, Kes1 LOF resulting in the licensing of nutrient-deprived cells to initiate and complete one extra cell division. Interestingly, accurate recapitulations of this *kes1Δ* phenotype, and of the premature entry into quiescence associated with excessive Kes1 activity, are apparent in complex developmental settings where exit from the cell cycle must be precisely timed. *Drosophila* embryonic cells lacking the Cdk inhibitor Dacapo undergo one extra cell division before the midblastula transition, whereas premature Dacapo expression induces G_1 arrest (de Nooij et al., 1996; Lane et al., 1996). Moreover, we also note the phenotypes of yeast expressing excessive Cln2 G_1 cyclin activity resemble *kes1*D cells in their ability to pass through G_1 in the face of severe nutrient deprivation (Hadwiger et al., 1989).

Sec14 and Kes1 Function at START in Cycling Cells

The Sec14/Kes1 signaling axis also operates in cycling cells at the commitment step before initiation of DNA replication. The larger critical size of *sec14–1*^{ts} cells indicates that these cells were unable to properly interpret that they had reached a sufficient size to commit to a new round of cell division. This defective coupling is qualitatively similar to that observed in cells deficient in the G_1 cyclin Cln3 and was corrected by Kes1 LOF. Hence, the Sec14/Kes1 axis not only regulates when cells stop dividing upon nutrient exhaustion, but also when cells initiate a new round of cell division in nutrient-rich conditions. Importantly, those interactions were evident in growing cells and without bulk membrane-trafficking deficits. Kes1 specificity in this level of control deserves emphasis. Other mechanisms for bypass Sec14 that correct the trafficking deficits associated with Sec14 LOF failed to correct the inability of *sec14–1*^{ts} mutants to properly register critical size. These results point to more specialized roles for Sec14/Kes1-regulated PtdIns-4-P-dependent signaling in cell-cycle control (Figure 7). This specific pool relevant to cell-cycle control is either: (1) functionally distinct from other Sec14/Kes1-regulated PtdIns-4-P pool(s) dedicated to bulk membrane-trafficking functions, or (2) involves the same pool but cell-cycle control exhibits a higher threshold requirement for PtdIns-4-P signaling.

Kes1 Is a Key Non-histone Substrate for the NuA4 Lysine Acetyltransferase

The role of Kes1 as inhibitor of progression through the START checkpoint argues for tight regulation of its activity. One such mechanism involves lipid binding/exchange as Kes1 is a brake on TGN/endosomal PtdIns-4-P signaling. The strength of that brake is regulated by a

heterotypic sterol and PtdIns-4-P binding/exchange cycle that is itself responsive to the availability of these lipids on TGN/endosomal membranes (Mousley et al., 2012). Our data indicate a second mechanism that involves K_{109} acetylation (Figure 7). This modification is an inactivating one as determined by both *in vivo* and *in vitro* assays. Those defects are reconciled by the unmodified K_{109} side chain engaging a PtdIns-4-P molecule in the Kes1 lipid-binding pocket (de Saint-Jean et al., 2011).

Our data indicating that impaired activity of the NuA4 KAT complex enhanced Kes1 activity in cells, and that an unmodified K_{109} was required for those effects, argue that Kes1 is an important non-histone target for this enzyme complex. In that regard, synthetic genetic array studies identified strong interactions of NuA4 deficiencies with cell-cycle and membrane-trafficking mutants (Lin et al., 2008; Mitchell et al., 2008). Those interaction networks: (1) resemble those of Sec14 and Kes1 (Mousley et al., 2008), (2) establish that NuA4 potentiates PKA signaling (Filteau et al., 2015), and (3) show NuA4 depresses both expression of the Msn2/4 regulon and trehalase (Lindstrom et al., 2006; Mitchell et al., 2008). Such pleiotropic NuA4 interactions are interpreted to reflect broad alterations in the transcriptome as a result of deranged histone acetylation landmarks. We posit that these synthetic phenotypes also report NuA4-dependent modulation of Kes1 activity, which contributes to the role of NuA4 as global genetic “buffer” that governs cell fitness (Lin et al., 2008; Mitchell et al., 2008).

Mechanistic Implications for Kes1 Lipid-Exchange Activity

Regardless of whether one favors intermembrane lipid transfer models for Kes1 function (de Saint-Jean et al., 2011), or a lipid-exchange-dependent sensing mechanism that does not involve intermembrane lipid transfer (Mousley et al., 2012), there is general agreement that the Kes1 lipid-exchange cycle is intimately linked to its biological activity. Modulation of Kes1 activity by K_{109} acetylation has implications for how the Kes1 lipid exchange cycle relates to protein function in the cell.

The data also present a paradox that indicates we do not yet fully understand the details of Kes1 activity in cells. While $Kes1^{AcK109}$ was defective in the coupled sterol/PtdIns-4-P countercurrent assay *in vitro*, the non-acetylated $Kes1^{K109R}$ showed robust activity, with only modest reduction in PtdIns-4-P transfer. Yet, $Kes1^{K109R}$ was nonfunctional *in vivo*. Those data suggest: (1) that $Kes1^{K109R}$ represents a striking case where lipid transfer protein function has been uncoupled from lipid exchange, (2) that even modest defects in the PtdIns-4-P component of the heterotypic DHE/PtdIns-4-P exchange cycle are sufficient to render $Kes1^{K109R}$ biologically inactive, or (3) that $K_{109}R$ interferes with, as yet, unidentified protein:protein or protein:lipid interactions critical for Kes1 biological activity. Either way, those results do not easily fit with models invoking intermembrane Kes1 lipid transfer mechanisms driven solely by differential sterol/PtdIns-4-P gradients.

ORPs and Cell-Cycle Control

The long ORP Osh1 and short ORP Osh6 both exhibited features suggesting that these too operate as nutrient-regulated brakes on G_1 progression. Such Osh activities, while resembling those of Kes1, were not precise redundancies, as the corresponding phenotypes

were apparent in the face of Kes1 activity. Rather, we interpret the data to report specific roles for these ORPs (Figure 7). Osh1 localization to the nuclear/vacuolar junction (and localization of its mammalian ortholog ORP1L to nuclear/lysosomal junctions) is interesting given the role of lysosomal compartments in nutrient signaling (Kvam and Goldfarb, 2004; Johansson et al., 2007). Osh6 is a PtdIns-4-P- and phosphatidylserine-binding protein (Maeda et al., 2013). We speculate that Osh6 couples its differential lipid-binding activities to other inputs into cell-cycle control.

While the LOF of the short ORPs, Osh5 or Osh6, had no effect on replicative lifespan, Kes1 LOF (short ORP) or LOF of any of the three long ORPs (Osh1, Osh2, and Osh3) extended both mean and maximal replicative lifespan. Mechanisms underlying the long replicative and short chronological lifespan of strains lacking Kes1 remain to be determined. Candidate pathways include TOR signaling and activation of the Gcn4 transcription factor (Mousley et al., 2012), altered trafficking processes related to PtdIns-4-P signaling (Li et al., 2002), and altered cell-cycle dynamics. Evidence to suggest that membrane trafficking integrates cell size homeostasis and cell-cycle progression (Anastasia et al., 2012), and building evidence for the involvement of cyclin-dependent kinase Cdk1 in this process (McCusker and Kellogg, 2012), suggest other possibilities.

Finally, the data hold implications for ORP involvement in mammalian cell-cycle control from the perspective of balancing cell proliferation with differentiation. High expression of Kes1-like short ORPs in mammalian tissues rich in post-mitotic cells is at least consistent with such a view (Johansson et al., 2003). We suggest that ORPs offer flexible mechanisms for coordinating endosomal membrane-trafficking flux and PtdIns-4-P signaling with cell-cycle progression, senescence, and transition of actively dividing cells into programs of differentiation and post-mitotic life.

STAR★METHODS

CONTACT FOR REAGENT AND RESOURCE SHARING

Requests for resources, reagents or further information should be directed to and will be fulfilled by the Lead Contact, Vytas A. Bank-aitis (vytas@tamhsc.edu).

EXPERIMENTAL MODEL AND SUBJECT DETAILS

Yeast strain genotypes and plasmids are listed in Key Resources. Standard yeast-peptone-dextrose, synthetic complete media and lithium acetate transformation methods were used throughout (Cleves et al., 1991; Schaaf et al., 2008).

METHOD DETAILS

Expression Vectors—Yeast and bacterial expression plasmids are listed in Key Resources. The P_{tet}-*KES1* and sterol-binding deficient mutant P_{tet}-*kes1*^{Y97F} vector was generated as follows. *KES1* or *kes1*^{Y97F} and the tetracycline/doxycycline-responsive promoter were amplified by PCR (Q5® High-Fidelity DNA Polymerase kit, NEB #E0555S), using primers that includes homologous ends to each other and to the pRS415 vector (for P_{tet}-*KES1*) or pRS413 vector (for P_{tet}-*kes1*^{Y97F}). The linearized DNA sequences were

cloned together by homologous recombination using SLICE (Zhang et al., 2008). Cloned vectors were isolated and confirmed by PCR. Tetracycline/doxycycline-inducible expression of *KES1*or *kes1*^{Y97F} was confirmed by immunoblot.

RT-PCR—Total RNA (1mg) templated reverse transcription to generate cDNA (20ml final volume). Expression of *AXL2, CLB1, CLN1, CLN2,PCL1, PCL9, ECM33, SCW10, SRL1, YOX1, CYC7, HSP104, CTT1, GPG1, GAD1, HSP12, HSP30, HSP82, HSP78, GRE1, SSA3* and *SSA4* relative to *ACT1* was determined using 0.5ml cDNA fraction as template and gene specific oligonucleotides as primers and the SensiFast Sybr Lo-Rox Kit (Bioline). Reactions were performed using a VIIA 7 Real-Time PCR System (Applied Biosystems).

Glycogen and Trehalose Measurements—Glycogen and trehalose were measured as described by Parrou and François (1997). Ten OD_{600nm} of cells were incubated in 250µl of 0.25M Na_2CO_3 at 95°C for 4 hr. After this the solution was adjusted to pH 5.2 with 150µl 1M acetic acid and 600 µl of 0.2M sodium acetate. For glycogen, samples were incubated overnight with 2 U/ml of amyloglucosidase isolated from *Aspergillus niger* (Sigma Aldrich) at 57°C with constant agitation. For trehalose, samples were incubated overnight with 0.05 U/ml of trehalase (Sigma Aldrich) at 37°C. The glucose liberated from either glycogen or trehalose was determined by incubating 50µl of sample with 500µl of glucose oxidase reagent (Sigma) for 30 min at 37°C. The reaction was terminated with 500µl of 12M H_2SO_4 and the absorbance measured at 420 nm.

Zymolyase Resistance Measurements—Cell harboring YCp(P_{DOX}::*KES1*), YCp(P_{DOX} :: *KES1*^{Y97F}) or YCp(P_{DOX}::*kes1*^{K109A}) were cultured to OD_{600} < 0.05 in synthetic defined medium lacking uracil containing Dox. Cells were isolated, washed and cultured in synthetic defined medium lacking uracil ± Dox for 18 hrs to OD_{600} < 1.0. Zymolyase resistance assays were performed according to Newman et al. (2005). Cells were grown in synthetic defined medium lacking uracil in the presence or absence of Dox at 30°C for the indicated times. Cells were isolated and resus-pended in water at 1 OD_{600nm}/ml and incubated with zymolyase 20T (150µg/ml) (ICN Biomedicals) at 30°C for 5, 10, 20 and 30 minutes. Cell lysis was monitored by measurement the OD_{600} nm.

Cell Cycle Methods—Elutriation experiments and cell size measurements were performed as described by Hoose et al. (2012). For elutriation experiments, cells were grown in YPD (1% $^{w}/_{v}$ yeast extract, 2% $^{w}/_{v}$ peptone, 2% $^{w}/_{v}$ dextrose) to a cell density of 1–5 × 10^7 cells/ml and loaded onto an elutriator chamber at a pump speed of 37 ml/min spinning at 3200 rpm (Beckman J-6M/E centrifuge). During all the centrifugation steps, the temperature in the centrifuge was 25°C. The elutriated small daughter cells were collected at 2400 rpm centrifuge speed and 42 ml/min pump speed, in tubes kept on ice. The elutriated cells were recovered by centrifugation and re-suspended in fresh pre-warmed YPD medium, at a cell density of ca. 1 × 10^7 cells/ml. The elutriated cultures were then placed in a 30°C incubator and every 20 min we recorded their budding index and measured their cell size with a Beckman Z2 channelyzer. The geometric mean of the cell size of the population was recorded using the Accucomp software package of the instrument. Each cell size measurement represents the average of two technical duplicates taken at two different cell

dilutions. The smoothened cell size histograms shown are the splines of the corresponding raw data, generated with the R software package “lattice”.

Replicative lifespan assays were performed on YPD agar at 30°C by serial separations of daughter cells from mother cells using a manual micromanipulator equipped with a fiber-optic needle (Steffen et al., 2009).

Flow Cytometry—Yeast (5 OD_{600} units) were pelleted and fixed overnight in 70% (v/v) ethanol. Cells were washed with 1 ml of citrate buffer (50 mM sodium citrate, pH 7), briefly sonicated, resuspended in 1 ml of citrate buffer containing 0.25 mg/ml RNase A, and incubated overnight at 37°C. Cells were again washed in 50 mM sodium citrate, pH 7.0, resuspended in 1 ml of 50 mM sodium citrate, pH 7.0 containing 16 mg/ml of propidium iodide, and incubated at room temperature for 30 min. After a last wash in citrate buffer, cells were analyzed on a Beckman MoFlo flow cytometer.

Detection of Lysine Acetylation by Mass Spectrometry—Lysine-acetylated Kes1 were produced using the amber suppression method of Hsu et al. (2016) where *E. coli* were cultured in Terrific broth supplemented with 0.2% arabinose, 5mM nicotinamide and 5mM Nε-Acetyl-L-lysine, and protein production was induced with IPTG at 16°C. In total, 4mg of purified protein (Kes1 or $Kes1^{AcK109}$) were digested with trypsin overnight. Resulting samples were analyzed by LC-MS/MS and acetylation sites were identified using a Mascot search engine (Mitchell et al., 2008).

PtdIns-4-P Extraction Assays—Extraction of [^{14}P]-PtdIns-4-P was measured as described (Goto et al., 2016). Liposomes (400 nm) composed of phosphatidylcholine (PtdCho), lactosyl-phosphatidylethanolamine (PtdEtn) and [^{14}P]-PtdIns-4-phosphate (86:10:4 molmol) were prepared by extrusion in liposome buffer (25 mM HEPES [pH 7.4], 150 mM, NaCl and 1 mM EDTA) and pre-cleared by centrifugation at 15,000xg for 5 min at 4°C. Extraction was measured by combining the appropriate Kes1 protein (100 pmol) with liposomes (400 pmol of PtdIns-4-phosphate) and 3 μg BSA in liposome buffer. After incubation at 25°C for 30 min, assays were placed on ice, *R. communis* agglutinin was added (10 μg) for 10 min and liposomes were sedimented by centrifugation at 15,000xg at 4°C for 5 min. [^{14}P]-PtdIns-4-phosphate was measured in supernatant fractions and PtdIns-4-P extraction was corrected for non-specific extraction (mock).

Lipids and Liposome Preparation for DHE and PtdIns-4-P Transfer Assays—1,2-dioleoyl-*sn*-glycero-3-phosphocholine (DOPC), brain L-α-phosphatidylinositol-4-phosphate (PtdIns-4-P), 1,2-dioleoyl-*sn*-glycero-3-phosphoethanolamine-N-(5-dimethylamino-1-naphthalenesulfonyl) (DNS-PE), and 1,2-dipalmitoyl-*sn*-glycero-3-phosphoethanolamine-N-lissamine rhodamine B sulfonyl (Rhod-PE) were from Avanti Polar Lipids. Dehydroergosterol (DHE) was from Sigma Aldrich. The concentration of the DHE stock solution in methanol was determined by UV-spectroscopy using an extinction coefficient of 13,000 $M^{-1}.cm^{-1}$.

Lipids, stored in stock solutions in $CHCl_3$ or methanol, were mixed at the desired molar ratios. Solvent was removed in a rotary evaporator under vacuum. For lipid films containing

PtdIns-4-P, the mix was pre-warmed to 33°C for 5 minutes prior to drying. The films were hydrated in 50mM Hepes, pH 7.2, 120mM K-acetate (HK buffer) to obtain a suspension of multilamellar liposomes. After five thawing-freezing cycles with liquid nitrogen, the suspensions were extruded through polycarbonate filters of 0.2mm pore size using a mini-extruder (Avanti Polar Lipids). Liposomes were stored at 4°C in the dark when containing light-sensitive lipids (DHE, DNS-PE, Rhod-PE), and used within 2 days.

DHE and PtdIns-4-P Transfer Assays—DHE and PtdIns-4-P transport assays followed the protocols described (de Saint-Jean et al., 2011; Moser von Filseck et al., 2015) using purified recombinant His_6-tagged Kes1 proteins (Li et al., 2002). Experiments were carried out in a Shimadzu RF 5301-PC fluorimeter equipped with a cylindrical quartz cuvette. For measuring DHE transfer, a suspension (570µl) of L_B liposomes (200µM lipids, final concentration) made of DOPC and containing 4% (mol/mol) PtdIns-4-P was incubated at 30°C under constant stirring in HKM (HK + 1mM $MgCl_2$) buffer. After 1 min, 30µl of L_A liposomes (200µM lipid final concentration) composed of 2.5% of DNS-PE and 5% DHE was added. After 3 min, Kes1 or the appropriate derivative was injected to a final concentration of 375nM. Lipid transport was measured by recording the DNS-PE signal at 525nm (bandwidth 10 nm) upon DHE excitation at 310nm (bandwidth 1.5nm). As the concentration of accessible DHE was equal to 10µM, the amount of DHE (in µM) transported from L_A to L_B membrane was equal to $10 * ((F-F_0)/(F_{max}-F_0))$ where F_{max} is the signal before Kes1 injection; F_0 is the signal measured upon total DHE extraction by 10mM methyl-β-cyclodextrin (Sigma). Liposomes and proteins were injected from stock solutions with Hamilton syringes through a guide in the cover of the fluorimeter.

To measure PtdIns-4-P transport, a suspension (570µL) of L_B liposome (200µM total lipid) composed of 2% Rhod-PE and 4% PtdIns-4-P was incubated with 250nM NBD-PH_{FAPP} at 30°C in HKM buffer under constant stirring. The concentration of accessible PtdIns-4-P (in the outer leaflet) is 4µM. After 1 min, 30µL of L_A liposome containing 10% DHE (200µM lipids, final concentration) were injected. After additional 3 min, Kes1 or mutant (375nM final concentration) was injected. PtdIns-4-P transport was followed by measuring the NBD signal at 530 nm (bandwidth 10nm) upon excitation at 460nm (bandwidth 1.5nm). The signal, which mirrors the redistribution of NBD-PH_{FAPP} between L_A and L_B liposomes, was normalized to determinate the amount of PtdIns-4-P transported by Kes1. For this, the NBD signal (F_{eq}) in a situation where PtdIns-4-P is fully equilibrated between liposomes. NBD-PH_{FAPP} was mixed with L_A and L_B liposome (200µM total lipid each) that each contains initially 2% PtdIns-4-P. The fraction of PtdIns-4-P on the surface of L_B liposome, PtdIns-4-P_B/PtdIns-4-$P_{T,}$ is equal to the fraction of PH_{FAPP} on L_B liposome and correspond to $F_{Norm} = 0.5*(F-F_0/F_{eq}-F_0)$ with F_0 corresponding to the NBD signal prior to the addition of Kes1 protein. The amount of PtdIns-4-P (in µM) transferred from L_B to L_A liposomes corresponds to $4*F_{Norm}$.

Fluorescence Microscopy—For GFP imaging, cells were grown in synthetic defined medium lacking uracil in the presence or absence of Dox at 30°C. Cells were then fixed in 3.75% formaldehyde and immobilized on concanavalin A coated slides and examined at 25°C. The imaging system employed a CFI plan apochromat lambda 100x oil immersion

objective lens NA 1.45 mounted on a Nikon Ti-U microscope base (Nikon, Melville, NY) interfaced to a Photometrics CoolSNAP HQ2 high sensitivity monochrome CCD camera (Roper Scientific, Ottobrunn, Germany) or an Andor Neo sCMOS CCD camera (Andor Technology, Belfast, UK). A Lumen 200 Illumination System (Prior Scientific Inc., Rockland, MA.) was used in conjunction with a B-2E/C (465–495nm/515–555nm;EX/EM) or G-2E/C (528–553nm/590–650nm;EX/EM) filter set (Nikon, Melville, NY). Images were captured using the Nikon NIS Elements software package (Nikon, Melville, NY, version 4.10) and exported as .TIF files. Image analyses were performed using ImageJ (version 1.47t, National Institute of Health) and figures were constructed using Adobe Illustrator and Adobe Photoshop CS6 (version 15.0.0).

Metabolic Radiolabeling and CPY Immunoprecipitation—Yeast strains were grown in minimal media lacking methionine and cysteine to mid logarithmic phase (OD_{600nm} = 0.5) and radiolabeled with [^{35}S]-amino acids (Translabel; New England Nuclear; 100 μCi/ml). Chase was initiated by introduction of unlabeled methionine and cysteine (2 mM each, final concentration), and terminated by addition of trichloroacetic acid (5% w/v – final concentration). CPY was pulled down from clarified cell-free lysates with rabbit polyclonal anti-CPY serum and radiolabeled CPY were resolved by SDS-PAGE and visualized by autoradiography (Bankaitis et al., 1986).

QUANTIFICATION AND STATISTICAL ANALYSIS

Data were quantified and analyzed as described in detail in the figure legends, figures, Results, and Method Details in STAR Methods. Statistical methods used included Student's t-test and one-way ANOVA, values are given as mean ± standard deviation and confidence intervals are identified. Exact definitions of n are identified throughout.

Supplementary Material

Refer to Web version on PubMed Central for supplementary material.

ACKNOWLEDGMENTS

This work was supported by grants GM44530 from the NIH and BE-0017 from the Robert A. Welch Foundation to V.A.B. C.J.M. was supported by start-up funds from Curtin University, Faculty of Health Sciences. K.B. and M.K. were supported by grant MOP-142403 from the Canadian Institutes of Health Research and a Natural Sciences and Engineering Research Council (NSERC) of Canada Discovery Grant (to K.B.). L.D. was supported by an NSERC Canada Graduate Scholarship. N.M. and M.P. were supported by grant GM123139 from the NIH to M.P. and by Texas A&M University Agrilife funds. G.D. was supported by the Center National de la Recherche Scientifique. B.K.K. is an Ellison Medical Foundation Senior Scholar in Aging and was supported by NIH grant R01 AG043080. C.H. was supported by a postdoctoral fellowship from the Glenn Foundation for Medical Research, and N.D.R. was supported by Canadian Institutes of Health Research grant MOP-136809. V.A.B. dedicates this paper to the memory of H. Alex Brown, an outstanding scientist, an exactingly rigorous experimentalist, and a most generous colleague and friend.

REFERENCES

Anastasia A, Nguyen DL, Thai V, Meloy M, Doyon Y, MacDonough T, and Kellogg DR (2012). A link between mitotic entry and membrane growth suggests a novel model for cell size control. J. Cell Biol 197, 89–104. [PubMed: 22451696]

Auger A, Galarneau L, Altaf M, Nourani A, Doyon Y, Utley RT, Cronier D, Allard S, and Côté J (2008). Eaf1 is the platform for NuA4 molecular assembly that evolutionarily links chromatin

acetylation to ATP-dependent exchange of histone H2A variants. Mol. Cell Biol 28, 2257–2270. [PubMed: 18212047]

Bankaitis VA, Aitken JR, Cleves AE, and Dowhan W (1990). An essential role for a PL transfer protein in yeast Golgi function. Nature 347, 561–562. [PubMed: 2215682]

Bankaitis VA, Johnson L, and Emr SD (1986). Mutants that fail to properly target protein to the yeast vacuole. Proc. Natl. Acad. Sci. USA 83, 9075–9079. [PubMed: 3538017]

Bankaitis VA, Malehorn DE, Emr SD, and Greene R (1989). The *Saccharomyces cerevisiae SEC14* gene encodes a cytosolic factor that is required for transport of secretory proteins from the yeast Golgi complex. J. Cell Biol 108, 1271–1281. [PubMed: 2466847]

Bankaitis VA, Mousley CJ, and Schaaf G (2010). Sec14-superfamily proteins and the crosstalk between lipid signaling and membrane trafficking. Trends Biochem. Sci 35, 150–160. [PubMed: 19926291]

Bard F, and Malhotra V (2006). The formation of TGN-to-plasma membrane transport carriers. Annu. Rev. Cell Dev. Biol 22, 439–455. [PubMed: 16824007]

Beck T, and Hall MN (1999). The TOR signalling pathway controls nuclear localization of nutrient-regulated transcription factors. Nature 402, 689–692. [PubMed: 10604478]

Beh CT, Cool L, Phillips J, and Rine J (2001). Overlapping functions of the yeast oxysterol-binding protein homologues. Genetics 157, 1117–1140. [PubMed: 11238399]

Brachmann CB, Davies A, Cost GJ, Caputo E, Li J, Hieter P, and Boeke JD (1998). Designer deletion strains derived from *Saccharomyces cerevisiae* S288C: a useful set of strains and plasmids for PCR-mediated gene disruption and other applications. Yeast 14, 115–132. [PubMed: 9483801]

Cameroni E, Hulo N, Roosen J, Winderickx J, and De Virgilio C (2004). The novel yeast PAS kinase Rim 15 orchestrates G_0-associated antioxidant defense mechanisms. Cell Cycle 3, 462–468. [PubMed: 15300954]

Clarke AS, Lowell JE, Jacobson SJ, and Pillus L (1999). Esa1p is an essential histone acetyltransferase required for cell cycle progression. Mol. Cell. Biol 19, 2515–2526. [PubMed: 10082517]

Cleves AE, McGee TP, Whitters EA, Champion KM, Aitken JR, Dowhan W, Goebl M, and Bankaitis VA (1991). Mutations in the CDP-choline pathway for phospholipid biosynthesis bypass the requirement for an essential phospholipid transfer protein. Cell 64, 789–800. [PubMed: 1997207]

de Nooij JC, Letendre MA, and Hariharan IK (1996). A cyclin-dependent kinase inhibitor, Dacapo, is necessary for timely exit from the cell cycle during *Drosophila* embryogenesis. Cell 87, 1237–1247. [PubMed: 8980230]

de Saint-Jean M, Delfosse V, Douguet D, Chicanne G, Payrastre B, Bourguet W, Antonny B, and Drin G (2011). Osh4p exchanges sterols for phosphatidylinositol 4-phosphate between lipid bilayers. J. Cell Biol 195, 965–978. [PubMed: 22162133]

Di Como CJ, Chang H, and Arndt KT (1995). Activation of *CLN1* and *CLN2* G1 cyclin gene expression by *BCK2*. Mol. Cell. Biol 15, 1835–1846. [PubMed: 7891677]

Fang M, Kearns BG, Gedvilaite A, Kagiwada S, Kearns M, Fung MKY, and Bankaitis VA (1996). Kes1p shares homology with human oxysterol binding protein and participates in a novel regulatory pathway for yeast Golgi-derived transport vesicle biogenesis. EMBO J 15, 6447–6459. [PubMed: 8978672]

Filteau M, Diss G, Torres-Quiroz F, Dubé AK, Schraffl A, Bachmann VA, Gagnon-Arsenault I, Chrétien AÈ, Steunou AL, Dionne U, et al. (2015). Systematic identification of signal integration by protein kinase A. Proc. Natl. Acad. Sci. USA 112, 4501–4506. [PubMed: 25831502]

Georgiev AG, Sullivan DP, Kersting MC, Dittman JS, Beh CT, and Menon AK (2011). Osh Proteins regulate membrane sterol organization but are not required for sterol movement between the ER and PM. Traffic 12, 1341–1355. [PubMed: 21689253]

Glick BS, and Nakano A (2009). Membrane traffic within the Golgi apparatus. Annu. Rev. Cell Dev. Biol 25, 113–132. [PubMed: 19575639]

Goto A, Charman M, and Ridgway ND (2016). Oxysterol-binding protein activation at endoplasmic reticulum-Golgi contact sites reorganizes phosphatidylinositol 4-phosphate pools. J. Biol. Chem 291, 1336–1347. [PubMed: 26601944]

Graham TR, and Burd CG (2011). Coordination of Golgi functions by phosphatidylinositol 4-kinases. Trends Cell Biol. 21, 113–121. [PubMed: 21282087]

Hadwiger JA, Wittenberg C, Richardson HE, de Barros Lopes M, and Reed SI (1989). A family of cyclin homologs that control the G1 phase in yeast. Proc. Natl. Acad. Sci. USA 86, 6255–6259. [PubMed: 2569741]

He C, Tsuchiyama SK, Nguyen QT, Plyusnina EN, Terrill SR, Sahibzada S, Patel B, Faulkner AR, Shaposhnikov MV, Tian R, et al. (2014). Enhanced longevity by ibuprofen, conserved in multiple species, occurs in yeast through inhibition of tryptophan import. PLoS Genet. 10, e1004860. [PubMed: 25521617]

Henriksen P, Wagner SA, Weinert BT, Sharma S, Bacinskaja G, Rehman M, Juffer AH, Walther TC, Lisby M, and Choudhary C (2012). Proteome-wide analysis of lysine acetylation suggests its broad regulatory scope in *Saccharomyces cerevisiae*. Mol. Cell. Proteomics 11, 1510–1522. [PubMed: 22865919]

Hoose SA, Rawlings JA, Kelly MM, Leitch MC, Ababneh QO, Robles JP, Taylor D, Hoover EM, Hailu B, McEnery KA, et al. (2012). A systematic analysis of cell cycle regulators in yeast reveals that most factors act independently of cell size to control initiation of division. PLOS Genet. 8, e1002590. [PubMed: 22438835]

Hsu WW, Wu B, and Liu WR (2016). Sirtuins 1 and 2 are universal histone deacetylases. ACS Chem. Biol 11, 792–799. [PubMed: 26820517]

Im YJ, Raychaudhuri S, Prinz WA, and Hurley JH (2005). Structural mechanism for sterol sensing and transport by OSBP-related proteins. Nature 437, 154–158. [PubMed: 16136145]

Johansson M, Bocher V, Lehto M, Chinetti G, Kuismanen E, Ehnholm C, Staels B, and Olkkonen VM (2003). The two variants of oxysterol binding protein-related protein-1 display different tissue expression patterns, have different intracellular localization, and are functionally distinct. Mol. Biol. Cell 14, 903–915. [PubMed: 12631712]

Johansson M, Rocha N, Zwart W, Jordens I, Janssen L, Kuijl C, Olkkonen VM, and Neefjes J (2007). Activation of endosomal dynein motors by stepwise assembly of Rab7-RILP-p150Glued, ORP1L, and the receptor βIII spectrin. J. Cell Biol 176, 459–471. [PubMed: 17283181]

Johnston GC, Pringle JR, and Hartwell LH (1977). Coordination of growth with cell division in the yeast *Saccharomyces cerevisiae*. Exp. Cell Res 105, 79–98. [PubMed: 320023]

Krause SA, and Gray JV (2002). The protein kinase C pathway is required for viability in quiescence in *Saccharomyces cerevisiae*. Curr. Biol 12, 588–593. [PubMed: 11937029]

Kvam E, and Goldfarb DS (2004). Nvj1p is the outer-nuclear-membrane receptor for oxysterol-binding protein homolog Osh1p in *Saccharomyces cerevisiae*. J. Cell Sci 117, 4959–4968. [PubMed: 15367582]

Lane ME, Sauer K, Wallace K, Jan YN, Lehner CF, and Vaessin H (1996). Dacapo, a cyclin-dependent kinase inhibitor, stops cell proliferation during *Drosophila* development. Cell 87, 1225–1235. [PubMed: 8980229]

Lester RL, Withers BR, Schultz MA, and Dickson RC (2013). Iron, glucose and intrinsic factors alter sphingolipid composition as yeast cells enter stationary phase. Biochim. Biophys. Acta 1831, 726–736. [PubMed: 23286903]

Li X, Rivas MP, Fang M, Marchena J, Mehotra B, Chaudhary A, Feng L, Prestwich GD, and Bankaitis VA (2002). Analysis of oxysterol binding protein homologue Kes1p function in regulation of Sec14p-dependent protein transport from the yeast Golgi complex. J. Cell Biol 157, 63–77. [PubMed: 11916983]

Lin YY, Qi Y, Lu J, Pan X, Yuan DS, Zhao Y, Bader JS, and Boeke JD (2008). A comprehensive synthetic genetic interaction network governing yeast histone acetylation and deacetylation. Genes Dev. 22, 2062–2074. [PubMed: 18676811]

Lindstrom KC, Vary JC, Jr., Parthun MR, Delrow J, and Tsukiyama T (2006). Isw1 functions in parallel with the NuA4 and Swr1 complexes in stress-induced gene repression. Mol. Cell. Biol 26, 6117–6129. [PubMed: 16880522]

Lillie SH, and Pringle JR (1980). Reserve carbohydrate metabolism in *Saccharomyces cerevisiae*: responses to nutrient limitation. J. Bacteriol 143, 1384–1394. [PubMed: 6997270]

Madsden CT, Sylvesteren KB, Young C, Larsen SC, Poulson JW, Andersen MA, Palmqvist EA, Hey-Morgensen M, Jensen PB, Treebak JT, et al. (2015). Biotin starvation causes mitochondrial protein

hyperacetylation and partial rescue by the SIRT3-like deacetylase Hst4p. Nat. Commun 6, 7726. [PubMed: 26158509]

Maeda K, Anand K, Chiapparino A, Kumar A, Poletto M, Kaksonen M, and Gavin A-C (2013). Interactome map uncovers phosphatidylserine transport by oxysterol-binding proteins. Nature 501, 257–261. [PubMed: 23934110]

McCusker D, and Kellogg DR (2012). Cdk1 coordinates cell-surface growth with the cell cycle. Curr. Opin. Cell Biol 24, 845–851. [PubMed: 23141634]

Mitchell L, Lambert J-P, Gerdes M, Al-Madhoun AS, Skerjanc IS, Figeys D, and Baetz K (2008). Functional dissection of the NuA4 histone acetyltransferase reveals its role as a genetic hub and that Eaf1 is essential for complex integrity. Mol. Cell. Biol 28, 2244–2256. [PubMed: 18212056]

Moser von Filseck J, Vanni S, Mesmin B, Antonny B, and Drin G (2015). A phosphati-dylinositol-4-phosphate powered exchange mechanism to create a lipid gradient between membranes. Nat. Commun 6, 6671. [PubMed: 25849868]

Mousley CJ, Tyeryar K, Ile KE, Schaaf G, Brost RL, Boone C, Guan X, Wenk MR, and Bankaitis VA (2008). Trans-Golgi network and endo-some dynamics connect ceramide homeostasis with regulation of the unfolded protein response and TOR signaling in yeast. Mol. Biol. Cell 19, 4785–4803. [PubMed: 18753406]

Mousley C, Yuan P, Gaur NA, Trettin KD, Nile AH, Deminoff S, Dewar BJ, Wolpert M, Macdonald JM, Herman PK, et al. (2012). A sterol binding protein integrates endosomal lipid metabolism with TOR signaling and nitrogen sensing. Cell 148, 702–715. [PubMed: 22341443]

Newman HA, Romeo MJ, Lewis SE, Yan BC, Orlean P, and Levin DE (2005). Gpi19, the *Saccharomyces cerevisiae* homologue of mammalian PIG-P, is a subunit of the initial enzyme for glycosylphosphatidylinositol anchor biosynthesis. Eukaryot. Cell 4, 1801–1807. [PubMed: 16278447]

Parrou JL, and François J (1997). A simplified procedure for a rapid and reliable assay of both glycogen and trehalose in whole yeast cells. Anal. Biochem 248, 186–188. [PubMed: 9177741]

Pedruzzi I, Bürckert N, Egger P, and De Virgilio C (2000). *Saccharomyces cerevisiae* Ras/cAMP pathway controls post-diauxic shift element-dependent transcription through the zinc finger protein Gis1. EMBO J. 9, 2569–2579.

Ramachandran V, and Herman PK (2011). The cAMP-dependent protein kinase signaling pathway is a key regulator of P body foci formation. Genetics 187, 441–454. [PubMed: 21078689]

Ramachandran V, Shah KH, and Herman PK (2011). The cAMP-dependent protein kinase signaling pathway is a key regulator of P body foci formation. Mol. Cell 43, 973–981. [PubMed: 21925385]

Schaaf G, Ortlund E, Tyeryar K, Mousley C, Ile K, Woolls M, Garrett T, Raetz CRH, Redinbo M, and Bankaitis VA (2008). The functional anatomy of PL binding and regulation of PIP homeostasis by proteins of the Sec14-superfamily. Mol. Cell 29, 191–206. [PubMed: 18243114]

Schulz TA, and Prinz WA (2009). Sterol transport in yeast and the oxysterol binding protein homologue (OSH) family. Biochim. Biophys. Acta 1771, 769–780.

Sikorski RS, and Hieter P (1989). A system of shuttle vectors and yeast host strains designed for efficient manipulation of DNA in *Saccharomyces cerevisiae*. Genetics 122, 19–27. [PubMed: 2659436]

Soma S, Yang K, Morales MI, and Polymenis M (2014). Multiple metabolic requirements for size homeostasis and initiation of division in *Saccharomyces cerevisiae*. Microb. Cell 1, 256–266. [PubMed: 28357252]

Spellman PT, Sherlock G, Zhang MQ, Iyer VR, Anders K, Eisen MB, Brown PO, Botstein D, and Futcher B (1998). Comprehensive identification of cell cycle-regulated genes of the yeast *Saccharomyces cerevisiae* by microarray hybridization. Mol. Biol. Cell 9, 3273–3297. [PubMed: 9843569]

Stefan CJ, Manford AG, Baird D, Yamada-Hanff J, Mao Y, and Emr SD (2011). Osh proteins regulate phosphoinositide metabolism at ER-plasma membrane contact sites. Cell 144, 389–401. [PubMed: 21295699]

Steffen KK, Kennedy BK, and Kaeberlein M (2009). Measuring replicative life span in the budding yeast. J. Vis. Exp 10.3791/1209.

Swinnen E, Wanke V, Roosen J, Smets B, Dubouloz F, Pedruzzi I, Cameroni E, De Virgilio C, and Winderickx J (2006). Rim15 and the crossroads of nutrient signalling pathways in *Saccharomyces cerevisiae*. Cell Div. 1, 3–11. [PubMed: 16759348]

Wei M, Fabrizio P, Hu J, Ge H, Cheng C, Li L, and Longo VD (2008). Life span extension by calorie restriction depends on Rim15 and transcription factors downstream of Ras/PKA, Tor, and Sch9. PLoS Genet. 4, e13. [PubMed: 18225956]

Zaman S, Lippman SI, Zhao X, and Broach JR (2008). How *Saccharomyces* responds to nutrients. Annu. Rev. Genet 42, 27–81. [PubMed: 18303986]

Zhang F, Gaur NA, Hasek J, Kim SJ, Qiu H, Swanson MJ, and Hinnebusch AG (2008). Disrupting vesicular trafficking at the endosome attenuates transcriptional activation by Gcn4. Mol. Cell. Biol 28, 6796–6818. [PubMed: 18794364]

Highlights

- Kes1 is a key brake on progression through G_1 upon nutrient limitation
- Kes1 and Sec14 coordinate cell growth with initiation of cell division
- Kes1 is a key non-histone target for the NuA4 lysine acetyltransferase
- Yeast ORPs inhibit cell-cycle progression and regulate replicative lifespan

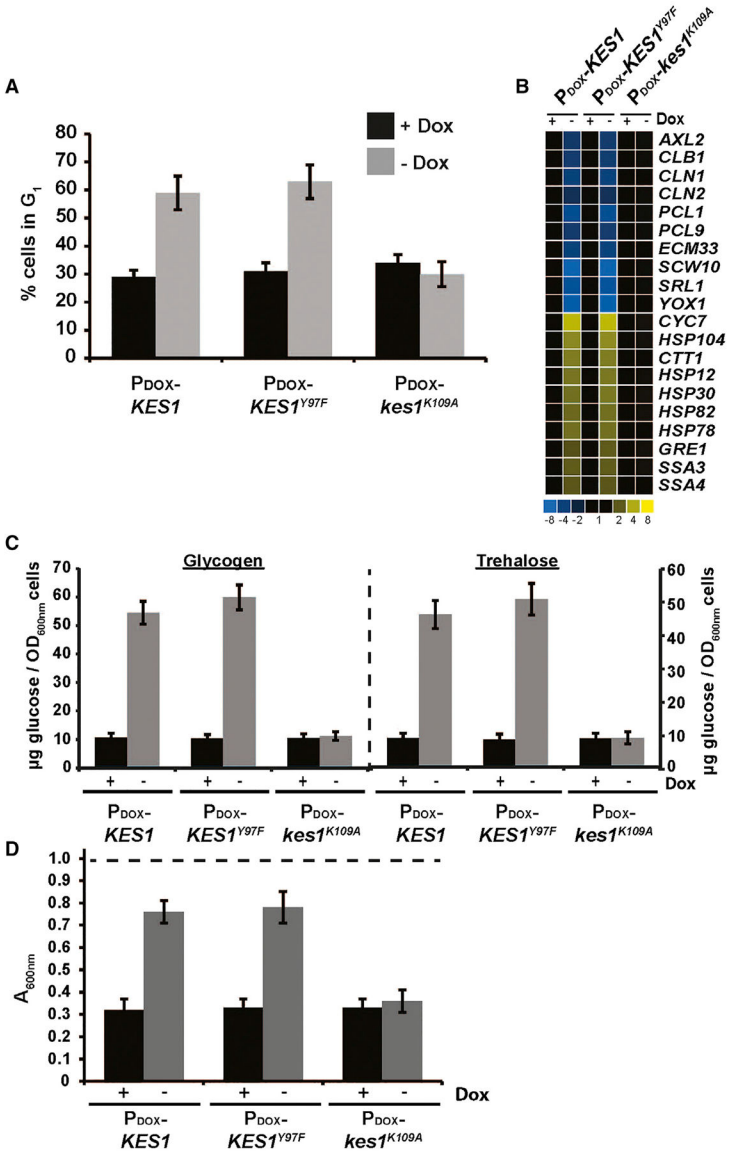

Figure 1. The Quiescence Response Is Activated upon Kes1-Induced Cell-Cycle Arrest

WT cells harboring the indicated plasmids were cultured in synthetic defined medium lacking uracil ± Dox as indicated. All experiments represent the averages of three independent biological replicates, and error bars indicate standard deviations.

(A) Asynchronous cultures were fixed and stained with propidium iodide and the cell-cycle distribution was determined based on genome content by fluorescence-activated cell sorting analysis. Plotted is the percentage of cells in G_1.

(B) Total RNA fractions were isolated and Msn2/4 and Gis1 target gene expression was surveyed by qRT-PCRand normalizedto*ACT1* gene expression.

(C) Glycogen and trehalose were extracted and hydrolyzed enzymatically to glucose with amylase and trehalase, respectively. Glucose was quantified and normalized per OD_{600} of cells.

(D) Cells were washed and resuspended in water to an initial density of OD_{600} of ~0.9 (starting OD_{600} indicated as dashed line at top) prior to treatment with zymolyase 20T (150 μg/mL) for 30 min. Cell lysis was assessed by scoring the reduction in the OD_{600} of the suspended cell cultures. See also Figures S1 and S2.

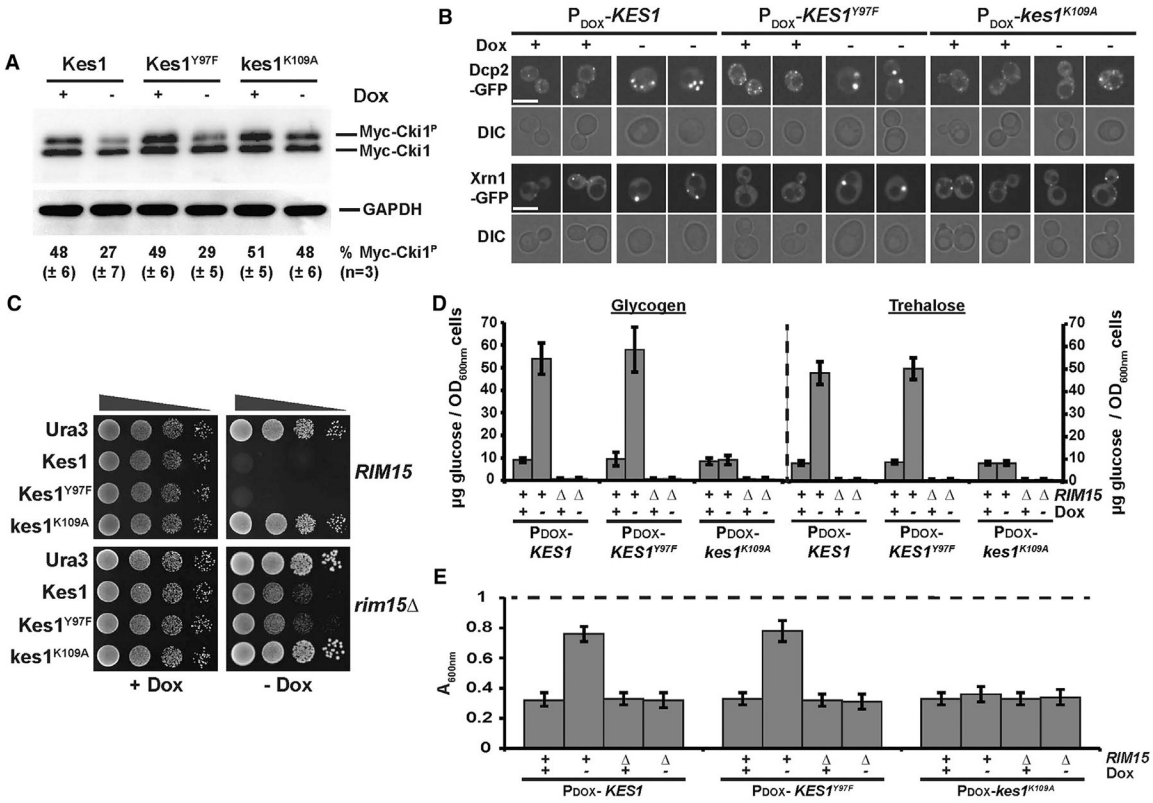

Figure 2. Kes1-Dependent Cell-Cycle Arrest Exhibits Reduced PKA Signaling and Is Rim15 Dependent

(A) Left panel: WT yeast co-transformed with YCp(*P_{CUP1}::myc-CKI1*), and either YCp(*P_{DOX}::KES1*), YCp(*P_{DOX} :: $KES1^{Y97F}$*), or YCp(*P_{DOX}::$kes1^{K109A}$*) were cultured in selective media containing 10 μg/mL Dox. Subsequently, *KES, $KES1^{Y97F}$*, or *$kes1^{K109A}$* expression was induced for 12 hr (–Dox), or not (+Dox; 10 μg/mL), and cells were challenged with $CuSO_4$ (100 μM for 1 hr) to induce myc-Cki1 expression. Lysates were prepared, normalized for total protein (10 μg loaded), and phosphorylated and non-phosphorylated myc-Cki1species and GAPDH were visualized by immunoblotting with anti-myc and anti-GAPDH antibodies, respectively. Phosphorylated and non-phosphorylated myc-Cki1species (myc-$Cki1^P$ and myc-Cki1, respectively) and GAPDH are identified on the left. Fractional proportion of phosphorylated myc-Cki1 as determined by densitometric analysis using image lab software (Bio-Rad) is shown at the bottom. Experiments represent the average of three independent biological replicates.

(B) Yeast cells expressing either Dcp2-GFP or Xrn1-GFP were transformed with the indicated plasmids and cultured in uracil-free medium ± Dox (10 μg/mL), as indicated, at 30°C. GFP profiles are shown with corresponding DIC images. Scale bar, 5 μm

(C) WT (BY4742) and isogenic *rim15Δ* cells carrying the indicated plasmids were spotted in 10-fold dilution series on uracil-free media ± Dox (10 μg/mL) and incubated at 30°C. Images were taken after 72 hr of incubation.

(D) Glycogen and trehalose were enzymatically hydrolyzed to glucose and quantified, as described in the legend to Figure 1C, in WT or *rim15Δ* cells harboring YCp(*P_{DOX}::KES1*),

YCp(P_{DOX} :: $KES1^{Y97F}$), or YCp(P_{DOX}::$kes1^{K109A}$), and cultured in synthetic defined medium lacking uracil ± Dox (10 μg/mL; black and gray bars, respectively).
(E) WT and *rim15*Δ yeast (as indicated), harboring YCp(P_{DOX}::*KES1*), YCp(P_{DOX} :: $KES1^{Y97F}$), or YCp(P_{DOX}::$kes1^{K109A}$) plasmids, were cultured in synthetic defined medium lacking uracil ± Dox (10 μg/mL) as indicated, washed, and resuspended in water to an initial density of OD_{600} of ~1.0 (starting OD_{600} depicted as dashed line at top) prior to treatment with zymolyase 20T (150 μg/mL). Cell lysis was assessed by scoring the reduction in the OD_{600} of the suspended cell cultures after 30 min of incubation. Data represent the average of three independent biological replicates.

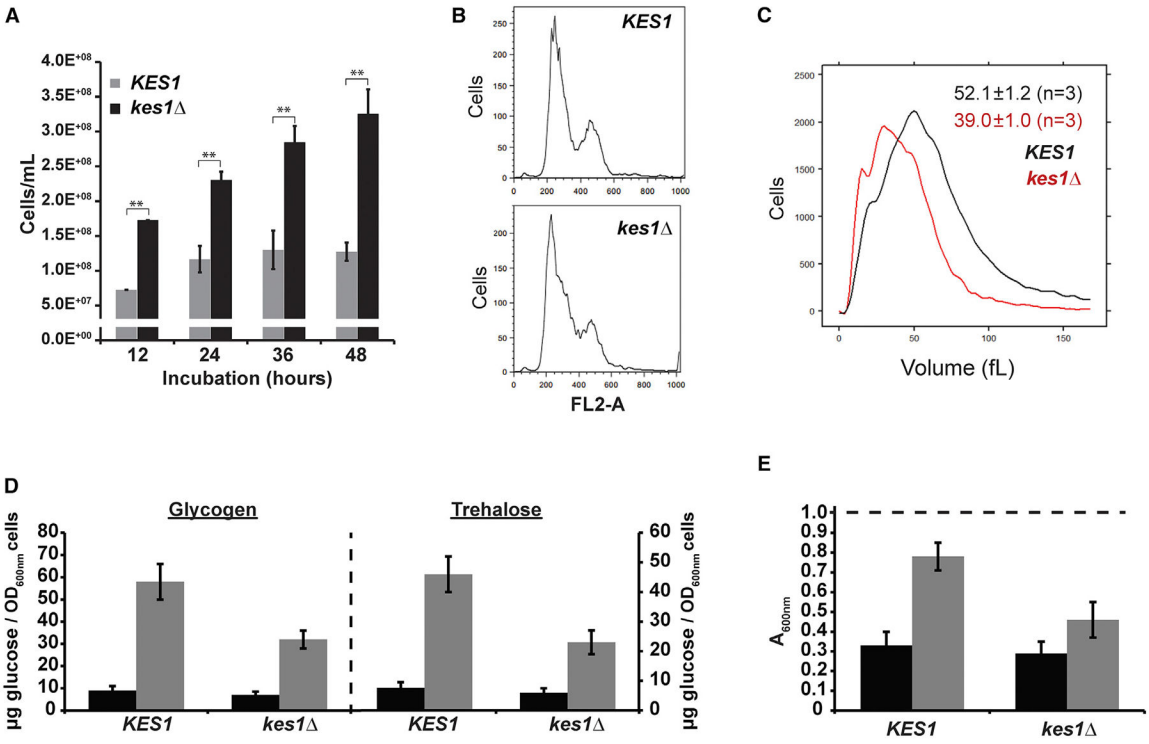

Figure 3. Cells Lacking Kes1 Respond Aberrantly to Nutrient-Restrictive Environments

Unless otherwise indicated, all experiments represent the averages of three independent biological replicates, and error bars indicate SDs.

(A) Cell densities of the indicated yeast strains (y axis) were quantified scored by light microscope hemacytometer counting at the indicated times as cells ceased to divide (x axis). Averages and standard deviations obtained from at least four independent experiments are shown. **p < 0.01, Student's t test.

(B) DNA content histograms of the indicated yeast strains collected at the 24 hr time point shown in (A) were generated by flow cytometry analyses. The number of cells analyzed in each case (y axis) is plotted as a function of fluorescence per cell (FL2-A; x axis).

(C) Cell size histograms of the indicated yeast strains collected at the 24 hr time point shown in (A) represent the distributions produced by channelyzer cell volume measurements (>30,000 individual cells measured per biological replicate). Cell number is plotted as a function of cell volume (in fL).

(D) Glycogen and trehalose were extracted from logarithmic (black bars) and stationary phase (gray bars) WT and *kes1Δ* cells grown in nutrient-rich media (YPD), hydrolyzed enzymatically to glucose, and glucose was quantified and normalized per OD_{600} cells.

(E) WT and *kes1Δ* yeast were cultured in YPD to logarithmic (black bars) and stationary phase (gray bars), washed and resuspended in water to a density of OD_{600} of ~0.9 (indicated as dashed line at top) prior to treatment with zymolyase 20T (150 μg/mL). Cell lysis was assessed by the reduction in the OD_{600} of suspended cell cultures after 30 min of incubation.

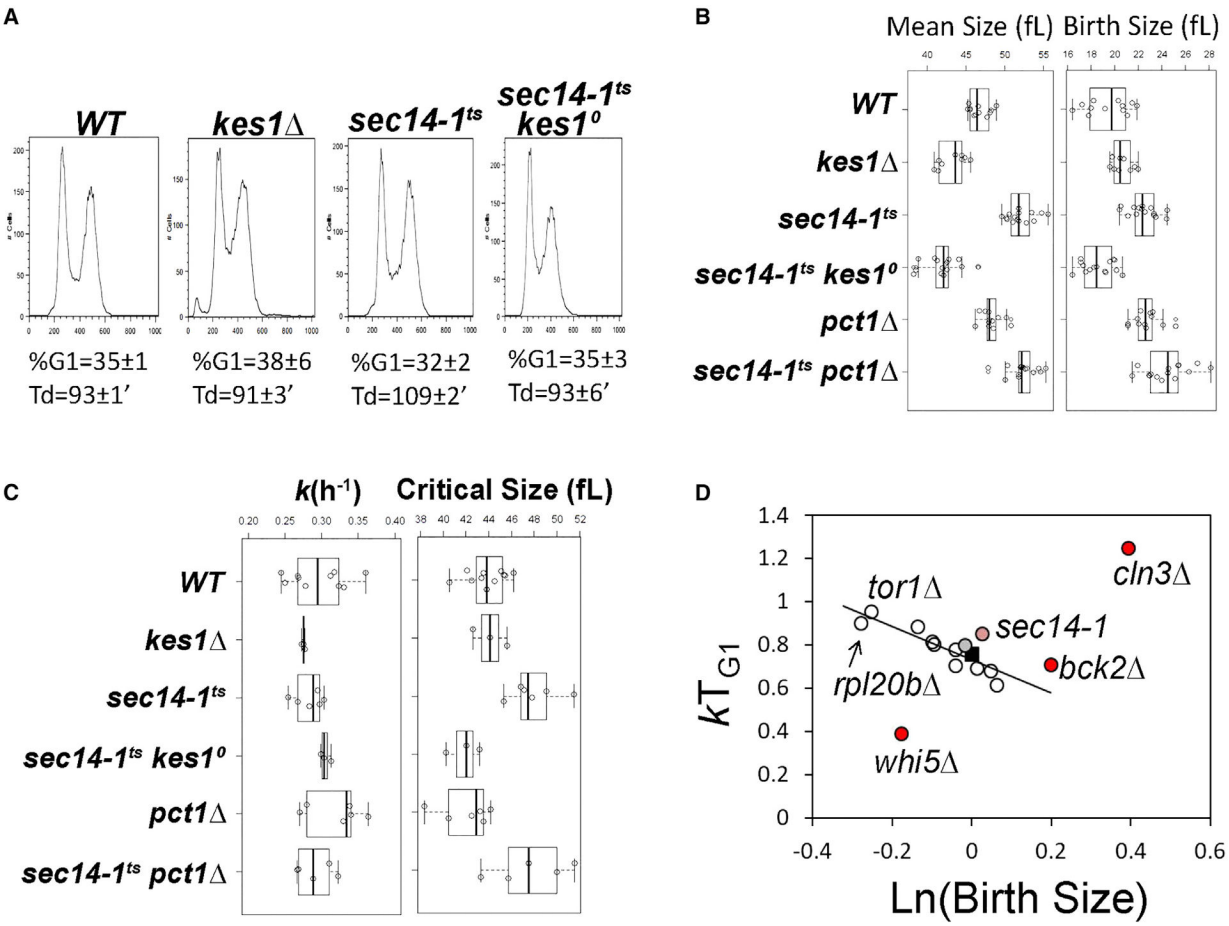

Figure 4. Mutual Antagonism of Kes1 and Sec14 in Cell-Cycle Control

(A) DNA content histograms were determined by flow cytometry. Fluorescence per cell (FL2-A) is plotted on the x axis, while the number of cells analyzed for each condition is plotted on the y axis. The average of the fractional representation of cells with G_1 content in the population (% G_1), and standard deviations (n = 6), are shown, along with the corresponding generation times (Td) in each case. Genotypes are identified at top.

(B) Boxplots reporting the mean and birth cell size (y axis, in fL) of asynchronously proliferating populations of yeast with the indicated genotypes. Each symbol (open circle) corresponds to an independent biological replicate where 30,000–150,000 individual cells were measured for each replicate.

(C) Boxplots depicting the specific rate of cell size increase, k (in hr^{-1}, left panel), and critical size (in fL, right panel) of synchronous cells of the indicated strains are shown.

(D) The relative growth in size during the G_1 phase (kT_{G1}, y axis) for the indicated mutants are plotted as a function of the natural logarithm of normalized birth size values (WT = 1). The line depicts the linear fit (obtained with the regression function of Microsoft Excel) of data from all mutants. Established cell-cycle regulator mutants are shown as controls (in red; *whi5*, defective in the repressor of passage through G_1; *cln3*, defective in a G_1 cyclin; *bck2*, a transcriptional activator of G_1 cyclins; previously reported in Soma et al., 2014). Values for WT (black square), the *sec14–1ts* mutant (light red), and *sec14–1ts kes1Δ* cells (gray) are highlighted.

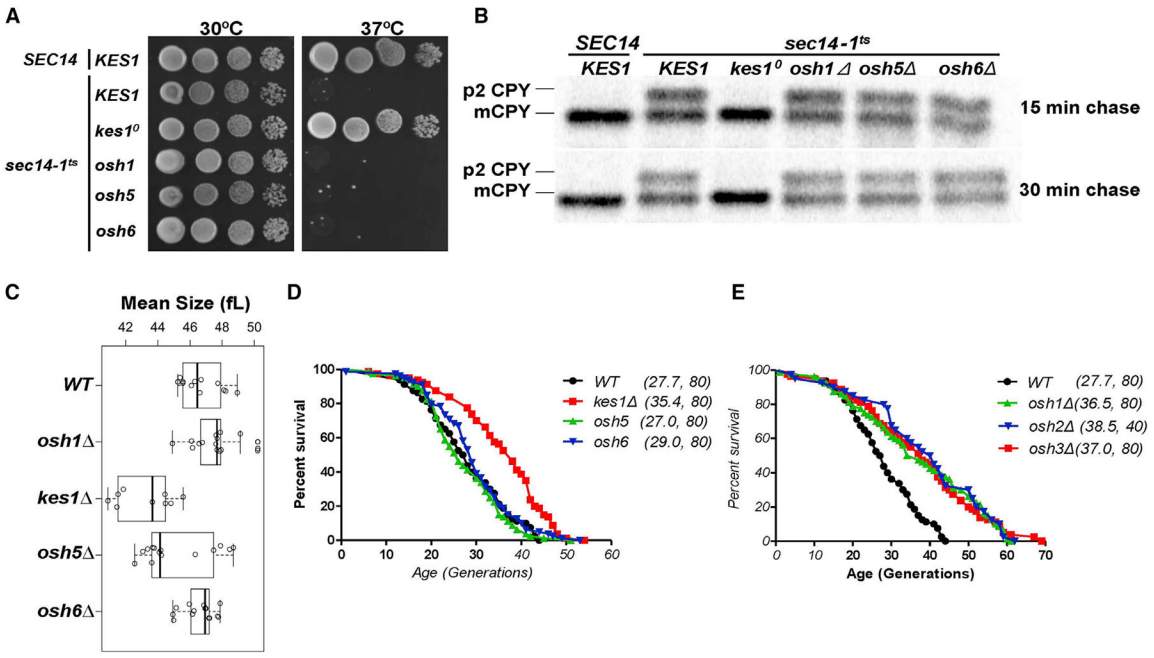

Figure 5. Functional Specification of Yeast ORPs

(A) *SEC14* or *sec14–1*^{ts} yeast (as indicated to the left of vertical line) with either a WT complement of yeast ORPs, or the indicated ORP deletion mutations (indicated to the right of the vertical line), were dilution spotted onto YPD agar and incubated at the indicated temperatures for 48 hr. Growth of *sec14–1*^{ts} derivative strains at 37°C identifies "bypass Sec14" phenotypes.

(B) Yeast strains of the indicated genotype (at top) were cultured to mid-logarithmic growth phase at 30°C, shifted to 37°C for 2 hr, and pulse-radiolabeled with [^{35}S]amino acids for 30 min. After chase with excess unlabeled methionine and cysteine for the indicated times (at right), CPY species were immunoprecipitated from clarified lysates, resolved by SDS-PAGE, and visualized by autoradiography. p2 CPY and mCPY forms are identified at the left.

(C) Boxplot reporting the mean cell size (in fL) of asynchronously proliferating populations of yeast with the indicated genotypes (at the left) in exponentially growing cultures. Each symbol (open circle) corresponds to an independent biological replicate consisting of 30,000–150,000 individual cells.

(D and E) Survival curves for *MAT*α *kes1Δ* cells (BY4742 derivative) cells (red), compared with otherwise isogenic and experiment-matched *KES1*$^{+}$ cells (black), and cells carrying individual deletions in the indicated genes encoding the short Osh proteins (*osh5Δ* cells, green; *osh6Δ*, blue) (D), and survival curves for *MAT*α *KES1* cells (black; BY4742) compared with otherwise isogenic and experiment-matched cells (black) carrying deletions in the indicated long Osh protein-encoding genes (*osh1Δ* cells, green; *osh2Δ*, blue; *osh3Δ*, red) (E). Mean lifespans are shown in parentheses, along with the number of cells assayed. See also Figure S3.

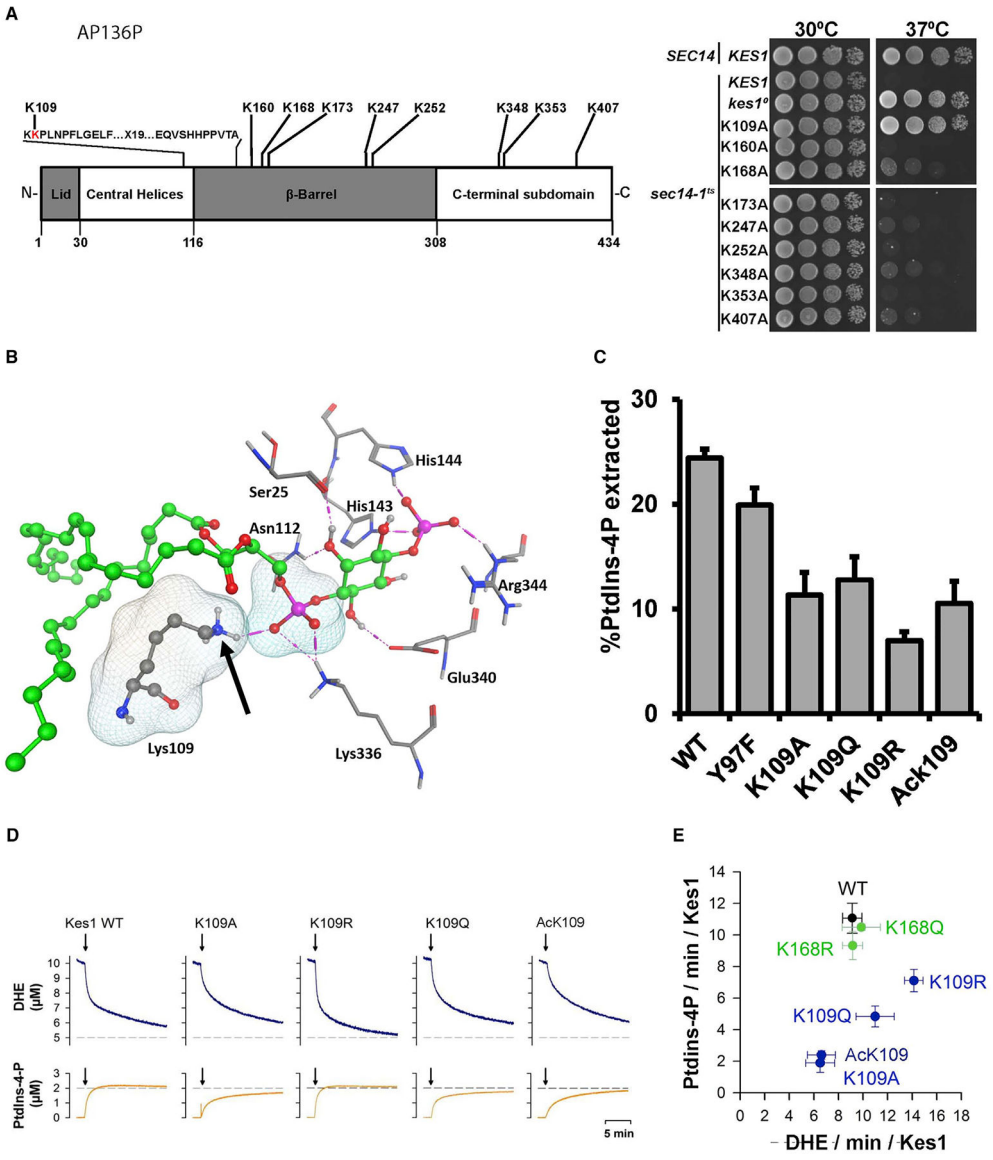

Figure 6. Functional Analyses of Kes1 Lysine Acetylation

(A) Top panel: schematic representation of Kes1 is shown. The ORP signature motif is highlighted (Li et al., 2002), as are the lysine acetylation sites identified by acetylome profiling (Henriksen et al., 2012; Madsden et al., 2015). Bottom panel: *SEC14* or *sec14–1^{ts}* yeast expressing Kes1, or the indicated K→A substitution mutants, were dilution spotted onto YPD agar and incubated at the indicated temperatures for 48 hr. The *SEC14 KES1* strain (positive control) and *sec14–1^{ts} KES1* (negative control at 37°C) are growth controls (two rows), the *sec14–1^{ts}, kes1^{0}* mutant defines the bypass Sec14 control (the *kes1^{0}* frameshift allele produces no Kes1 protein; third row).

(B) K_{109}A helps coordinate binding of the PtdIns-4-P head group. Kes1::PtdIns-4-P interactions are shown (PDB: 3SPW). Intermolecular H bonds between the PtdIns-4-P head group and the labeled Kes1 residues are shown by magenta dotted lines. PtdIns-4-P is rendered as green balls and sticks. Kes1 residues are shown in stick mode. Lys_{109} makes a

critical H bond interaction with the phosphate oxygen of PtdIns-4-P (van der Waals molecular surfaces shown). The Lys amino group modified by acetylation is marked by the arrow.

(C) PtdIns-4-P extraction activities for the indicated mutant/post-translationally modified Kes1 proteins were determined at 25°C in a 30 min endpoint format (see the STAR Methods). Mean ± standard deviations from three independent experiments are shown.

(D) Real-time DHE and PtdIns-4-P transport kinetics measured with Kes1 or versions bearing the indicated substitution for, or acetylation of, Lys_{109}. Top panel: DHE transport. Bottom panel: PtdIns-4-P transfer.

(E) Plot of initial DHE transfer rate versus initial PtdIns-4-P transfer rate for WT Kes1 and indicated mutant/post-translationally modified Kes1 proteins. Mean ± standard deviations from at least three independent experiments are shown. See also Figures S4–S7.

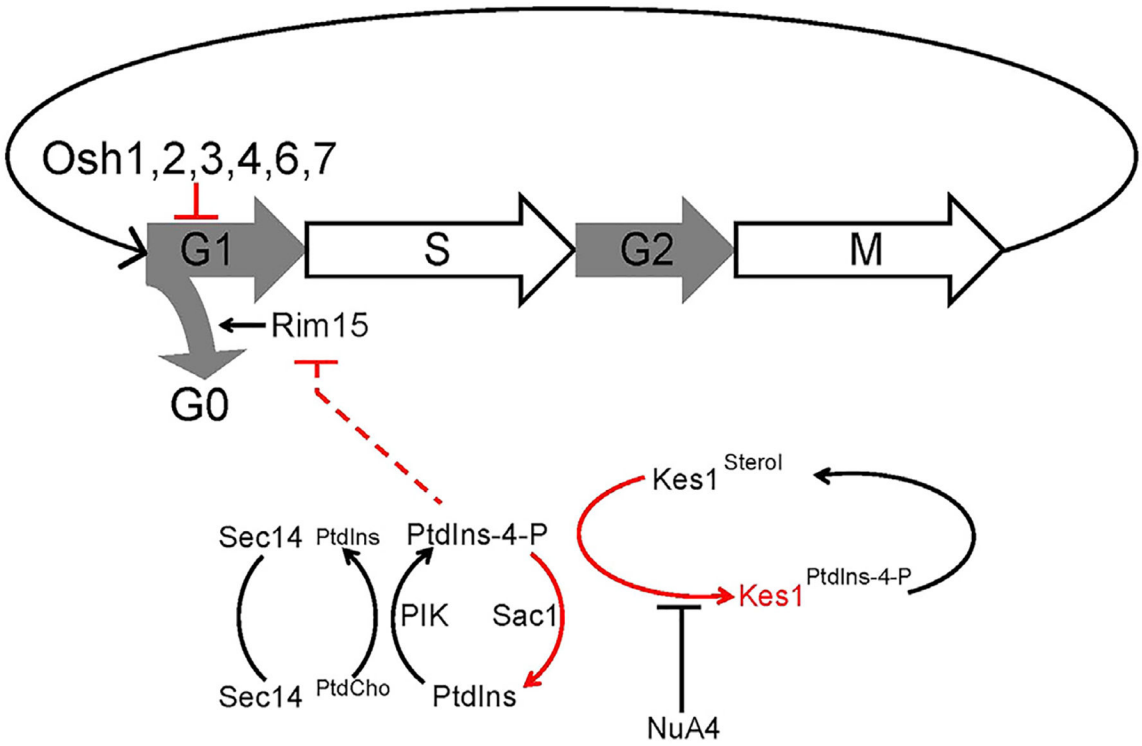

Figure 7. A Sec14/Kes1 PtdIns-4-P Signaling Axis in Cell-Cycle Control

Heterotypic PtdCho/PtdIns exchange defines the machine by which Sec14 stimulates PtdIns 4-OH kinase-mediated production of a PtdIns-4-P pool that regulates progression through the G_1 phases of the cell cycle. This signaling is antagonized by activity of the Sac1 PtdIns-4-P phosphatase and Kes1 binding and sequestering PtdIns-4-P from its effectors. The Kes1 brake is itself tuned by a heterotypic sterol/PtdIns-4-P exchange cycle and the activity of NuA4 KAT in acetylating K_{109}. The Sec14/Kes1 checkpoint requires activity of the Rim15 kinase, and we propose this PtdIns-4-P pool is produced in a TGN/endosomal compartment. Functionally distinct, roles for other Osh proteins (other than Osh5) in regulating G_1 progression are also indicated. Pathway brakes are highlighted in red.

KEY RESOURCES TABLE

REAGENT or RESOURCE	SOURCE	IDENTIFIER
Antibodies		
Rabbit polyclonal anti-CPY serum	Mousley et al. (2012)	RRID: AB_102312
Bacterial and Virus Strains		
BL21 (DE3)	New England Biolabs	BL21 (DE3)
Chemicals, Peptides, and Recombinant Proteins		
His_6-Kes1	Li et al. (2002)	N/A
His_6-Kes1^{K109A}	This study	N/A
His_6-Kes1 ^{K109Q}	This study	N/A
His_6-Kes1 ^{K109R}	This study	N/A
His_6-Kes1^{AcK109}	This study	N/A
Critical Commercial Assays		
SensiFast Sybr Lo-Rox Kit	Bioline	N/A
VIIA 7 Real-Time PCR System	Applied Biosystems	N/A
Q5 High-Fidelity DNA Polymerase kit	New England Biolabs #E0555S	N/A
Experimental Models: Organisms/Strains		
S. cerevisiae		
MATa, sec14-1, ura3-52, his3-200, lys2-801	Bankaitis et al. (1989)	CTY1-1A
MATa, sec14-1, pct1^0, ura3-52, his3-200, lys2-801	Cleves et al. (1991)	CTY102
MATa, sec14-1, kes1^0, ura3-52, his3-200, lys2-801	Fang et al. (1996)	CTY159
MATa, sec14-1, cki1-1, ura3-52, his3-200, lys2-801	Cleves et al. (1991)	CTY160
MATa, ura3-52, his3-200, lys2-801	Bankaitis et al. (1989)	CTY182
MATa, sec14-1, ura3-52, his3-200, lys2-801, cki1Δ::URA3	This study	CTY392
MATa, ura3-52, his3-200, lys2-801, cki1Δ::URA3	This study	CTY393
MATa, ura3-52, his3-200, lys2-801, pct1Δ::URA3	This study	CTY1784
MATa, ura3-52, his3-200, lys2-801, kes1Δ::URA3	This study	CTY1683
MATa, ura3-52, his3-200, lys2-801, cki1Δ::URA3	This study	CTY1784
CTY1683 *leu2Δ::KES1-3XFLAG::HIS3*	This study	JHY2
CTY1683 *leu2Δ::kes1 K109A-3XFLAG::HIS3*	This study	JHY3
CTY1683 *leu2Δ::kes1 K109Q-3XFLAG::HIS3*	This study	JHY4
CTY1683 *leu2Δ::kes1 K109R-3XFLAG::HIS3*	This study	JHY5
CTY159 *leu2Δ::KES1-3XFLAG::HIS3*	This study	JHY6
CTY159 *leu2Δ::kes1 K109A-3XFLAG::HIS3*	This study	JHY7
CTY159 *leu2Δ::kes1 K109Q-3XFLAG::HIS3*	This study	JHY8
CTY159 *leu2Δ::kes1 K109R-3XFLAG::HIS3*	This study	JHY9
CTY159 *leu2Δ::kes1 K168Q-3XFLAG::HIS3*	This study	JHY10
CTY159 *leu2Δ::kes1 K168R-3XFLAG::HIS3*	This study	JHY11
CTY182 *osh1Δ::URA3*	This study	JHY14
CTY182 *osh2Δ::URA3*	This study	JHY15
CTY182 *osh3Δ::URA3*	This study	JHY16

REAGENT or RESOURCE	SOURCE	IDENTIFIER
CTY182 *osh5Δ::URA3*	This study	JHY17
CTY182 *osh6Δ::URA3*	This study	JHY18
CTY182 *osh7Δ::URA3*	This study	JHY19
CTY1-1A *osh1Δ::URA3*	This study	JHY20
CTY1-1A *osh2Δ::URA3*	This study	JHY21
CTY1-1A *osh3Δ::URA3*	This study	JHY22
CTY1-1A *osh5Δ::URA3*	This study	JHY23
CTY1-1A *osh6Δ::URA3*	This study	JHY24
CTY1-1A *osh7Δ::URA3*	This study	JHY25
MATa his3Δ1 leu2Δ0 met15Δ0 ura3Δ0 DCP2-GFP::HIS3MX6	Invitrogen	CJM1
MATa his3Δ1 leu2Δ0 met15Δ0 ura3Δ0 XRN1-GFP::HIS3MX6	Invitrogen	CJM2
MATa his3Δ1 leu2Δ0 lys2Δ0 ura3Δ0rim15Δ::KanMX4	Dharmacon	CJM3
MATa his3Δ1 leu2Δ0 met15Δ0 ura3Δ0	Brachmann et al. (1998)	BY4741
MATa his3Δ1 leu2Δ0 lys2Δ0 ura3Δ0	Brachmann et al. (1998)	BY4742
MATa his3Δ1 leu2Δ0 met15Δ0 ura3Δ0 eaf1 Δ::KANMX	GE Life Sciences	YKB3333
MATa his3Δ1 leu2Δ0 met15Δ0 ura3Δ0 rtt109Δ::KANMX	GE Life Sciences	YKB3484
MATa his3Δ1 leu2Δ0 met15Δ0 ura3Δ0 elp3Δ::KANMX	GE Life Sciences	YKB3482
MATa his3Δ1 leu2Δ0 met15Δ0 ura3Δ0 gcn5Δ::KANMX	GE Life Sciences	YKB3489
MATa his3Δ1 leu2Δ0 met15Δ0 ura3Δ0 hat1 Δ::KANMX	GE Life Sciences	YKB3485
MATa his3Δ1 leu2Δ0 met15Δ0 ura3Δ0 sas2Δ::KANMX	GE Life Sciences	YKB3486
MATa his3Δ1 leu2Δ0 met15Δ0 ura3Δ0 sas3Δ::KANMX	GE Life Sciences	YKB3487
MATa his3Δ1 leu2Δ0 met15Δ0 ura3Δ0 hpa2Δ::KANMX	GE Life Sciences	YKB3488
MATa his3Δ1 leu2Δ0 met15Δ0 ura3Δ0 hpa3Δ::KANMX	GE Life Sciences	YKB3297
MATa his3Δ1 leu2Δ0 met15Δ0 ura3Δ0 sec14^{ts}-NATMX eaf1Δ::KANMX	This study	YKB3935
MATa his3Δ1 leu2Δ0 met15Δ0 ura3Δ0 sec14^{ts}-NATMX rtt109Δ::HIS3	This study	YKB4074
MATa his3Δ1 leu2Δ0 met15Δ0 ura3Δ0 sec14^{ts}-NATMX elp3Δ::KANMX	This study	YKB3444
MATa his3Δ1 leu2Δ0 met15Δ0 ura3Δ0 sec14^{ts}-NATMX gcn5Δ::KANMX	This study	YKB4080
MATa his3Δ1 leu2Δ0 met15Δ0 ura3Δ0 sec14^{ts}-NATMX hat1Δ::KANMX	This study	YKB3442
MATa his3Δ1 leu2Δ0 met15Δ0 ura3Δ0 sec14^{ts}-NATMX sas2Δ::KANMX	This study	YKB3447
MATa his3Δ1 leu2Δ0 met15Δ0 ura3Δ0 sec14^{ts}-NATMX sas3Δ::KANMX	This study	YKB3449
MATa his3Δ1 leu2Δ0 met15Δ0 ura3Δ0 sec14^{ts}-NATMX hpa2Δ::KANMX	This study	YKB4065
MATa his3Δ1 leu2Δ0 met15Δ0 ura3Δ0 sec14^{ts}-NATMX hpa3Δ::KANMX	This study	YKB3451
MATa his3Δ1 leu2Δ0 met15Δ0 ura3Δ0 eaf7Δ::KANMX	This study	YKB3292
MATa his3Δ1 leu2Δ0 met15Δ0 ura3Δ0 esa1 Δ::HIS3 esa1^{ts}-URA3	GE Life Sciences	YKB4236
MATa his3Δ1 leu2Δ0 met15Δ0 ura3Δ0 sec14^{ts}-NATMX eaf7Δ::KANMX	This study	YKB4068
MATa his3Δ1 leu2Δ0 met15Δ0 ura3Δ0 sec14^{ts}-NATMX esa1Δ::HIS3 esa1^{ts}-URA3	This study	YKB4242
Recombinant DNA		
Plasmids		
YCp(HIS3)	Sikorski and Hieter (1989)	pRS413
pEVOL (*mmAcKRs, araC*)	Hsu etal. (2016)	pEVOL-MmAcKRS
YCp(LEU2)	Sikorski and Hieter (1989)	pRS415

REAGENT or RESOURCE	SOURCE	IDENTIFIER
pRS413 *Ptet::KES1^{Y97F}*	This study	pKB302
pRS415 *Ptet::KES1*	This study	pKB321
YCp(*URA3, P_{dox}::KES1*)	Mousley et al. (2012)	pCJM1
YCp(*URA3, P_{DOX}:: KES1^{Y97F}*)	Mousley et al. (2012)	pCJM2
YCp(*URA3, P_{DOX}:: kes1^{K109A}*)	Mousley et al. (2012)	pCJM3
pRS313 Cki1$^{1-200}$:: Myc$_{6x}$*HIS3*	Ramachandran and Herman (2011)	pPHY2328
pQE30 (*KES1*)	Li et al. (2002)	pRE540
pQE30 (*KES1^{Y97F}*)	This study	pRE1454
pQE30 (*kes1^{K109A}*)	This study	pJH1
pQE30 (*kes1^{K109Q}*)	This study	pJH2
pQE30 (*kes1^{K109R}*)	This study	pJH3
pQE30 (*kes1^{K109amber}*)	This study	pJH4
pQE30 (*KES1^{K168Q}*)	This study	pJH5
pQE30 (*KES1^{K168R}*)	This study	pJH6
pDR196(*GFP-SNC1, URA3*)	This study	pJH7
Software and Algorithms		
Nikon NIS Elements software package version 4.10	Nikon, Melville, NY	N/A
ImageJ version 1.47t	National Institute of Health	N/A
Accucomp Beckman Z2 channelyzer software package	Beckman Instruments	N/A
R software package “Lattice”	Trellis Graphics (Cleveland, OH)	Lattice graphics